Final Report

Output 7 - Medical devices including in vivo/in vitro trials and exome analysis

Completion date: 30/06/2021

Dennis Douroumis

University of Greenwich

Corresponding detail: d.douroumis@greenwich.ac.uk

This project has received funding from the Interreg 2 Seas programme 2014-2020 co-funded by the European Regional Development Fund under subsidy contract 2S01-059_IMODE.

OUTPUT 7	Medical devices including in vivo/in vitro trials and exome analysis
Project specific objective	Innovative medical devices with improved therapeutical activity based on co-drugs
Output description	Prototypes of 3D printed stents and also metal stents coated with biodegradable and biocompatible polymers optimized.
Project Output Target	1
Expected project specific result (s)	New prototype: new medical devices prototypes with property of prolonged delivery of co-drugs (expected gain 80% in delivery) elaborated from advanced techniques for the treatment of coronary artery diseases. The developed devices will be ready to use for biomedical applications. They will increase the competitiveness of biomedical SMEs and generate job creations. 1 Patent is targeted
Partner responsible	University of Greenwich
Other Partners involved	University of Lille, Imabiotech, Ashford and St Peter's Hospital's NHS Foundation Trust

Summary of the objectives, activities and achievements obtained during the project

Stents are medical devices used to revascularize a stenosed artery. Following the implantation of a stent, a new occlusion (restenosis) appeared in half of the cases. The first generations of stents using non-degradable polymers reduced restenosis but caused late thrombosis due to excessive inflammation caused by erosion of the polymer. The second generation solved partially these problems by proposing absorbable polymers, new molecules and better control of the drug release. However, the problem remains in 5% of cases for the gold standard of the coronary stent and no effective solution exists for the peripheral arteries. The objective of the IMODE project is to develop and evaluate stents to improve the treatment of patients in both coronary and peripheral arteries.

The first strategy introduced by the University of Greenwich is to fabricate a bioresorbable drug eluting stent comprising of biocompatible polymer blends such as polylactic acid and polydioxanone containing a flavonoid (antiproliferative agent). This was done by using a 3D printing technology called Fusion Deposition Modelling where printable polymer filaments are fed into the printer's nozzle to fabricate the stent design. The technology allows the fabrication of several stent designs and the combination of various polymer blends or drug substances incorporated in the stent strut. The mechanical properties and the printing optimization of the various systems have been

investigated and the printed stents could be crimped and expanded without any defects on a balloon catheter.

The second strategy consisted of depositing an electrospun absorbable (chitosan / cyclodextrin polymer) or non-absorbable (polyurethane) membrane containing simvastatin on the metallic stents by the UMET-ISP team from University of Lille. The electrospinning process parameters have been optimized for both strategies. This consisted to define the instruments settings of the electrospinning machine and those of the electrospun solution in order to realize the coating of the metallic stent with membranes made of nanofibers (NFs). Two prototypes of active stents could be prepared bearing membranes with well defined thicknesses and NFs diameters capable of delivering the efficient dose of simvastatin within a prolonged delay. The functional specifications were also respected, as the coated stent could be inserted inside the catheter used for positioning the stent in the arteria during the angioplasty surgical act. The prototypes, after their in vitro evaluation (cytocompatibility, hemocompatibility, drug release kinetic) have been transferred to the group of U1008 for pre-clinical tests.

The stents were evaluated on a rabbit model developed by the University of Lille. First, the hypercholesterolemic animal model was developed with a bare metal stent (BMS) and a Drug Eluting Stent (DES) on the market. Briefly, the rabbits received a diet enriched in cholesterol (D0); a balloon injury is made in the artery to create the stenosis (J7), a stent is then implanted (J42), the stent is then evaluated 28 days after surgery. The results showed significant thromboses on the stents containing the electrospun PCD / CHT / SV membrane whereas the stents containing the electrospun PUR / SV membrane behaved like an active stent on the market. 3D printed stents are under evaluation.

A more complete analysis of the drug inside the arteries was carried out by Imabiotech. By using MALDI Mass Spectrometry Imaging, ImaBiotech has investigated the distribution of simvastatine in the different layers of the artery wall after removal of a simvastatine-loaded stent made by electrospinning. The images revealed the presence of SV in media and adventice until 24h with an exposure of media five times less exposed than the adventice. Maximum concentration observed in tissue was 350 µg/g in media at 1.5h.

Finally, a study was carried out by Ashford and St. Peter's Hospitals NHS Foundation. In order to clarify the genetic basis of vascular disease in the brain related to stenosis, the partner was able to recruit over 800 subjects with cerebral venous thrombosis, a condition that mimics stroke and affects young females. Detailed demographic information was acquired including age of onset and the majority of the known risk factors. DNA was subsequently extracted and an whole genome search was undertaken. A single locus was identified associated with this form of stenosis. The region lies in the ABO blood group region. Further, genetic analysis determined that those with AB blood group were 5 times more susceptible to cerebral veno-vascular disease compared to non-O blood group. This work has important implications for understanding the causes of blood vessel stenosis.

Description of the scientific and technological achievements

1. INTRODUCTION

Cardiovascular pathologies are a major challenge of public health whose risk factors are on the rise. The chronic arterial aggression lead to atherosclerosis, responsible stroke, myocardial infarction and chronicle lower limb ischemia. Several endovascular procedures have been developed, such as angioplasty and stenting, with minimally invasive surgery, that is more appropriate for old and precarious patients. However, their medium- and long-term results remain to be improved. They are limited by in-stent restenosis and early in-stent thrombosis, related to local cellular response and inflammatory phenomena. In order to avoid RIS, several stents coated with antimitotic drugs (Drug Eluting Stent - DES) have been developed, but their clinical efficacy is not always the desired. Over the last 10 years research focuses on the development of new DES to prevent local inflammatory phenomena that appear after stenting. The aim of this work was to develop DES prototypes with property of prolonged delivery of co-drugs elaborated from advanced techniques, and to create and validate an animal model to test these DES candidates. In addition, we introduced the engineering and development of bioresorbable drug eluting stents fabricated using 3D printing technology. The 3D printed stents can be personalized according to the patient needs by adjusting the length, strut thickness, geometry of the design, type drug loaded and dissolution profiles varying from 1-3 months.

2. MATERIALS AND METHODS

2.1. Materials

Chitosan (CHT; 69 000 g/mol; 98.26 % deacetylated, Wisapple Beijing), polyethylene oxide (PEO; 900 000 g/mol, Sigma Aldrich), glacial acetic acid (AA, Sigma Aldrich), Hydroxypropyl β-cyclodextrin polymer (PCD), Polyurethane (TPU; Elastollan® 1185A, Mw=79 kDa, USP Class VI, BASF, Germany), N,N-Dimethylformamide (DMF, Sigma Aldrich), Tetrahydrofuran (THF, Sigma Aldrich), hydroxypropyl β-cyclodextrin (HPβCD, SD = 0.62, Roquette, France), citric acid (CA) and simvastatin (SV, Farmalabor). All reagents were used as received from the manufacturer without further purification. Ultrapure water was used for all the experiments (Veolia water aquadem, Purelab flex, ELGA, 18.2 MV).

2.2. Drug eluting stents manufacturing

2.2.1. Chitosan based nanofibers preparation

Chitosan based nanofibers were fabricated by dissolving PCD (33.3 wt%) and SV (33.3 wt%) in 90 % (v/v) acetic acid aqueous solution (90 v/v - %). The mixture was kept under stirring at 350 rpm for 15 minutes. 33.3 % wt of CHT and PEO powder mixture (9:1) (w/w) were then added to the solution and left under stirring at 450 rpm overnight until homogenization. The polymer solution was loaded into a 5 mL syringe placed onto a syringe pump (Fisher Scientific) operating with a flow rate of 0.3 mL/h and joined with 21-gauge needle (BD, USA) by the intermediate of polyethylene perfusion extension (inner diameter 1 mm; VYGON). Nanofibers were deposited on aluminium tubes (L40 x D5.5 mm) or stents and fixed onto a rotative collector (speed 200 rpm). The distance between the needle and the collector is fixed at 20 cm and the applied voltage is fixed to 13 – 17 kV. The electrospinning procedure lasts 30 minutes and was carried out in an insulated cell where the temperature and humidity were controlled (22 ± 2 °C and 27 ± 2% respectively). The nanofibrous samples were then transferred to a vacuum oven at 90 °C overnight or at 120 °C for 4 hours in order to evaporate the residual solvent in the nanofibers.

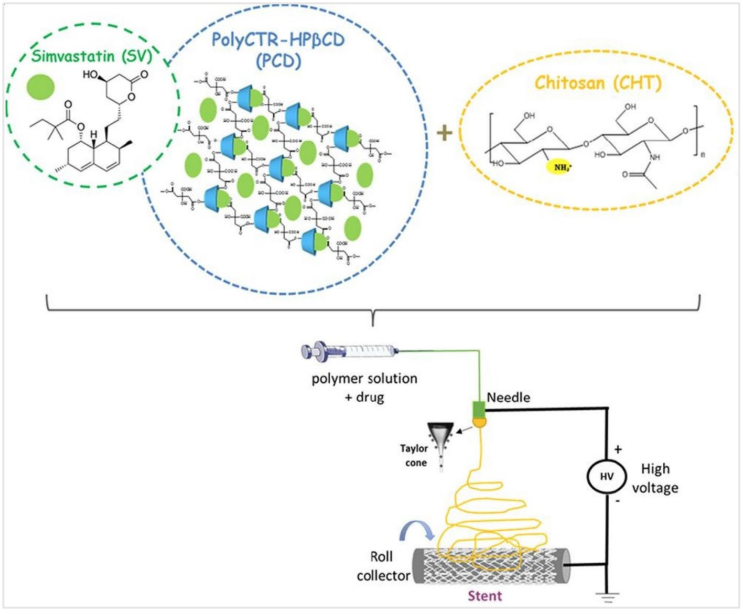

Figure 1: elestrospinning process, example of a stent made of chitosan based nanofibers.

2.2.2. Polyurethane based nanofibers preparation

Polyurethane based nanofibers were prepared by dissolving 10 % (w/v) of TPU in a solvent mixture containing DMF and THF (2:3) (v/v) and 5% w/v of SV were incorporated in the polymer solution. It was left under stirring at 550 rpm during 60 minutes. The same methodology was used but the electrospinning procedure lasts 45 minutes and its parameters were as follow: flow rate of 0.5 ml/h, distance of 20 cm and an applied voltage of 8 to 10 kV, temperature 22 ± 2 °C, relative humidity of 27 ± 2% and collector rotation speed at 200 rpm.

2.2.3. Hot melt extrusion

The various PDO/PLA physical blend were prepared and mixed using a turbula shaker-mixer (Glen Mills T2F Shaker/Mixer). Physical blend was fed into the hopper of a single- screw hot melt extruder (Filabot EX6, Filabot HQ, USA). The extrusion temperature across the screw was set 35^{o}C, 160^{o}C, 170^{o}C and 140^{o}C. The physical blend was extruded using a 1.8- and 2.5-mm circular dies. The extruded filaments were passed through a cooling system consisting of 5 cooling fans and collected using a filament winder. The filament winding speed was adjusted to generate a filament with a desired diameter ranging from 1.6-1.8 and 2.6-2.9 mm respectively.

2.2.4. Computer aided design (CAD) of stent

The stent model used for the printing optimisation experiments was a novel, cylindrical based stent with closed, chevron- shaped cells (figure 2.1). The stent designs in figure 2.1 were designed using the commercial CAD software, SolidWorks 2016 (Dassault Systèmes). All Solidworks files were exported as STL files prior to transfer to the slicing software.

2.2.5. 3D printing of bioresorbable stents

The 3D printer chosen for manufacture of the stent design, for this experiment and subsequent experiments, was the Ultimaker 3 Extended (Ultimaker Ltd, Geldermalsen, Netherlands). The Ultimaker 3 Extended is a bowden tube style printer which has its feeder gears locate stationary at the back of the printer and its liquefier/hot-end located in the print head, this is as opposed to some other FDM printers which incorporate the feeder and liquefier at the print head. Prior to printing, in order to make the file readable to the printer, the STL files were converted to .Gcode files using the 3D printer slicing software, Cura (Version 3.3.1) (Ultimaker Ltd, Geldermalsen, Netherlands). The aim of the work

was to analyse the manufacturing processes of the printer and to see the effects of three pre-selected parameters on the dimensional accuracy of the printed item, therefore, all parameters were kept constant but the parameter being tested.

For the experiments, a custom bought print core (UM3 HardCore Pro) was fitted with a 0.15 mm diameter micro nozzle both purchased from 3D Solex (3D Solex, Norway). Upon switching the 3D printer on, build plate active levelling and XY calibration of the print head was carried out. Prior to each print the build plate of the printer was cleaned with acetone and active levelled. To ensure the nozzle was free from blockage with damaged PLA filament the nozzle was allowed to extrude material to clear debris, this was done using the print core cleaning function on the printer. After, hot pull cleaning was carried out and led to even material extrusion, the cleaning PLA filament was removed from the print head and the printer was set up again for subsequent printing. Nozzles found to be blocked with PLA after the hot pull were soaked in acetone until the filament could be removed from inside. Grinding of the filament was rectified by opening the feeder section of the printer and cleaning of the polymer dust from the feeder gears. The gnawed section of filament was removed from the spool and the filament was reloaded after closure of the feeder compartment. Dual extrusion was not used for the printing and all stents were printed using the extruder on the left of the print head

2.2.6. Stents crimping

Balloon-expandable stents made of Chrome Cobalt (Multi-Link 8 LL, Coronary Stent System, Abbott, USA) and autoexpansible stents made of NiTinol (Zilver Flex, COOK® medical, USA) were used. Their diameters were between 2 and 3 mm for in vivo experiments, 3 to 6 mm for in vitro experiments. All data were reported to the surface of the electrospun membrane (unit mass / μm^2). Before electrospinning, the stent was released from its delivery system, and was threaded on the mandrel collector in its expanded form. After the NFs deposition, in order to ensure that covered stents are still compliant with the angioplasty surgical act, they must be re-conditioned inside the delivery catheter. Therefore, a crimper apparatus (HV200 transcatheter heart valve crimping tools, MSI, USA) **(Figure 2)** was used for constricting the stent and re-introduce it inside the catheter.

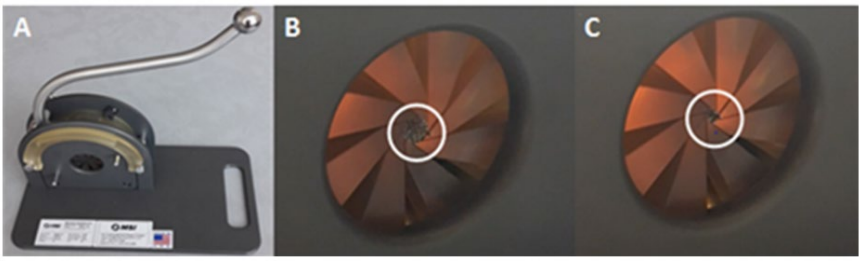

Figure 2. (A) Image of crimper apparatus, (B) and (C) stent crimping.

2.2.7. NFs characterization

The NFs morphology was examined using a scanning electron microscope (SEM, Higuchi S-4700 SEM field emission GU, Japon) operating at an accelerating voltage of 5 kV and an emission current of 10 µA. All samples were sputtered beforehand with a thin layer of platinium (100 Å) before analysis.

2.3. Biological evaluation

These tests were performed following the International and European standards (ISO 10993-5/EN 30993-5) with the human pulmonary microvascular endothelial cell line (HPMEC-ST1.6R).The cells were cultured in endothelial cell growth medium MV (PromoCell GmbH, Heidelberg, Germany) enriched with endothelial cell growth supplement (PromoCell GmbH, Heidelberg, Germany), streptomycin (0.1 g/L), and penicillin (100 IU/mL), at 37 °C in a CO2 incubator (CB 150/APT line/ Binder, LabExchange, Paris, France) with 5% CO2/ 95% atmosphere and 100% relative humidity.

2.3.1. Drug release assay

In vitro release study of simvastatin was performed in dynamic conditions using a fully automated flow through cell dissolution apparatus (SOTAX UPS, CE7 smart with CP7 piston pump, Switzerland) operating in a closed loop configuration. Stents loaded with SV were placed into flow cells (n=6). Drug release profiles were monitored in PBS / SDS (0.7 % v/v) (SDS) at pH 7.4 circulated at a constant flow rate (35 mL/min) under a constant temperature (37 °C). A fixed volume of PBS/SDS was withdrawn at different time intervals, then placed in vials and analyzed by high pressure liquid chromatography (HPLC, SHIMADZU 2010C-HT, Gemini C18 5 µm x 150 mm (Phenomenex)) to determine the amount of SV released until 24h. The mobile phase used was a 30:70 (v/v) mixture of Potassium dihydrogen

phosphate (KH_2PO_4, 3.5 g/L, pH 4.5, Sigma Aldrich) and acetonitrile pumped at a flow rate of 0.8 mL/min. The analysis was performed at 30 °C and the detection wavelength fixed at 238 nm.

2.3.2. Cytotoxicity assay (extract dilution method)

The nanofibers were weighted and placed, for extraction purposes, into complete culture medium (CCM) in a ratio of 6 cm²/ml for 72 h at 37◦C under agitation at 80 rpm (Innova40, New Brunswick Scientific, France). In parallel, 4.0 × 10^3 HPMEC cells per well were seeded in a 96-welltissue culture plate containing 100 µL of CCM per well. After 72 h, the extraction medium was collected and sterile-filtered (0.2 mL PB Acrodisc®; PALL, France). The culture medium was removed from the cells and 100 µl/well of the filtrated extraction medium or CCM (negative control), i.e. absence of cytotoxicity, were respectively added to the wells. After 24 h of incubation, the cell viability was measured by the AlamarBlue®assay (ThermoFisher Scientific, France). Briefly, extraction medium was removed from the cells and 200 µl/well of a 10% AlamarBlue® in CCM solution were added to the wells and placed, protected from light, in an incubator for2 h. Then, 150 µl of the AlamarBlue® solution were recovered from each well and transferred into a flat bottom 96-well plate. Fluorescence was measured at an excitation wavelength of 530 nm and an emission wavelength of 590 nm, on a microplate fluorometer (TwinkleTMLB 970; Berthold Technologies GmbH & Co, Germany). The fluorescence readings were normalized relative to that of the negative controls. The experiments were performed in triplicate.

2.3.3. Cytocompatibility assay

The growth period for cell proliferation tests was 3 days with no renewal of the culture medium. Nanofibers sample, cut in 15 mm diameter disks were placed in 24-well plates (Falcon, Corming) with a Viton ring (Radiospares) to maintain the samples on the bottom of the wells and subsequently to avoid cell growing beneath the test samples. 10000 cells were gently seeded in each well and placed in the CO2 incubator. Cell viability was assessed with the non-toxic Alamar Bluedye (Interchim). Three and six days after the cell seeding, the culture medium was removed from each well and 500 mL of diluted Alamar Blue dye were added to each sample. After 3 hours of incubation, 100 mL of this solution were transferred into a 96- well plate (Nunc Polylabo) and the fluorescence was measured with a fluorometer (Twinkle LB970TM, Berthold, France) at an excitation wavelength of 510 nm and an emission wavelength of 590 nm. Data were expressed as the mean percentage ± SD of six separate experiments with respect to the control (Tissue Culture PolyStyrene, TCPS – 100 %).

1.1. In vivo assay

All animal experiments were approved by the Ethics Committees on animal testing (CEEA ; European directive 2010/63). Adult male New Zealand white rabbits (SEGAV, St Mars-D'Egrenne, France) were housed in an individual cage in a temperature and light controlled room. The rabbits were fed with fat diet (0.3% cholesterol and 4.9% coconut oil) for 7 weeks, followed by a normal feeding (SSNIFF, Soest, Germany). A treatment with acetylsalicylic acid (ASA) 20 mg/day was administered in the drinking water all the protocol long. All operations were carried out under general anaesthetic inducted by 1mL intra-muscular injection of Xylazine and 1 mL of Ketaminend and then maintained by 2.5% isoflurane combined with oxygen at tracheal mask for the entire duration of the procedure (1 L/min). At the end of the protocol, rabbits were anesthetized according to the same protocol. A median laparotomy was performed and the sub-renal aorta and the iliac axes were dissected. The sub-renal aorta was punctured using a 22 G needle and an arteriogram (DSA) by manual injection of 5 mL of Xenetix 300 (Guerbet, Villepinte, France) was performed to estimate the permeability and degree of stenosis of the iliac arteries. The sub-renal aorta was ligated and the iliac arteries (with ou without stents) were harvested and then fixed in 4% paraformaldehyde (PAF). Rabbits were euthanized at the end of the surgery by injection of 2 mL of phenobarbital T61 in the heart. A summary of procedures is presented in **Figure 3.**

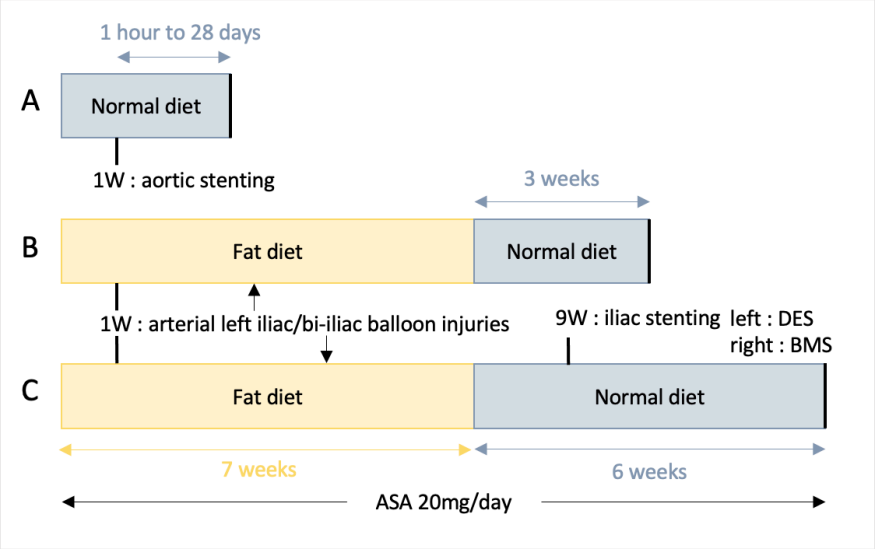

Figure 3. In vivo pharmacokinetic (A), rabbit model protocol validation (B) and first application (C) : arterial injuries are created unilaterally (B) or bilaterally (C), acetylsalicylic acid (ASA) is administred in all cases all protocol long

2.3.4. In vivo pharmacokinetics analysis (Fig. 3A)

2.3.4.1. Biological sample preparation

To assess the diffusion of SV in the arterial wall, non-hypercholesterolemic rabbits were used. A treatment with acetylsalicylic acid (ASA) 20 mg/day was administered in the drinking water all the protocol long. Diet remained normal throughout the protocol and no arterial damage was achieved (figure 3A). After 1 week of normal diet, rabbits were anesthetized using the same protocol as describe previously. After shaving both inguinal area and disinfection with biseptin, an incision was made in the inguinal fold in order to control each femoral artery. After puncture of femoral artery with a needle (18G), a 4-French introducer sheath (Radiofocus TIF TIP, TERUMO Tokyo, Japon) was inserted into the vessel, preloaded with a guide wire TERUMO 0,035' (Radiofocus, TERUMO, Tokyo, Japon). Then, 100 UI/kg heparin was administrated via the introducer device. Aorta was catheterized with a 0.018' guide wire and each animal received one PCD-CHT-SV stent in the sub-renal aorta. One rabbit received a BMS as controlled, and one received a PU-SV stent. Rabbits should have been sacrificed at the 1st or the 6th hour, at the 1st, 7th, 14th and 28th postoperative day according to the same protocol for euthanasia. Only the sub-renal aorta was harvested and samples were sent to ImaBiotech to quantify the distribution of SV using MALDI - Mass Spectrometry Imaging (MSI). This study will determine the amount of SV in the media (composed of smooth muscle cells) at different defined times and thus determine the release profile of simvastatin from NFs in vivo.

2.3.4.2. MALDI Mass Spectrometry Imaging

2.3.4.2.1. Sectioning

Ten micrometer-thick cryosections of each artery sample (except time point 4h, too damaged by stent removal) have been obtained at -20°C using a HM560 cryostat (Thermo Scientific, Germany) and mounted on ITO conductive glass slides (Delta Technologies, Loveland, USA). The slides were stored at -80°C until analysis by MALDI MSI. Low resolution image of the slide was also obtained using a scanner (Epson Perfection V330 Photo, France).

2.3.4.2.2. MALDI matrix application

After an initial drying step under vacuum, the slide is coated with a MALDI matrix. Method development for simvastatine has led to the conclusion that 40 mg/mL 2,5-dihydroxybenzoic acid

(DHB) in MeOH:water 1:1 v:v + 0,1% trifluoracetic acid (Sigma-Aldrich, Saint Quentin Fallavier, France) was the best choice to achieve optimal sensitivity. DHB matrix was deposited on the slide using an TM automatic sprayer (HTX Technologies, Chapel Hill, NC, USA).

2.3.4.2.3. Histological staining

Histological staining using Hematoxylin-Eosin (H&E) has been performed either on section images by MALDI Imaging after matrix removal with 100% methanol or on adjacent sections. High-definition images were obtained with a digital slide scanner 3D Histech Panoramic.

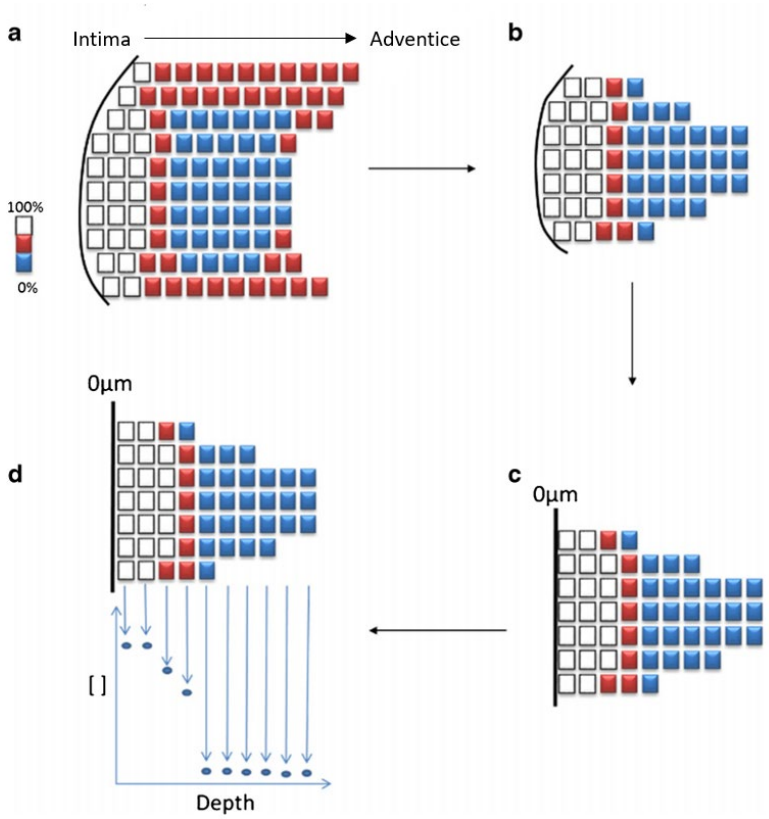

Figure 4: Scheme of the different steps to build a depth profile with Multimaging software, including selection of a region of interest, extraction of the raw data per pixel, alignment of the pixel lines, quantification of each line and display as a function of distance from lumen

2.3.4.2.1. Quantification

Quantification has been performed by spotting on the ITO slide 1 µL droplets of calibration solutions of simvastative from 25nM to 1mM in MeOH:water. In order to account for the tissue extinction effect, the Tissue Extinction Coeficient (TEC) approach has been used. TEC are obtained homogeneously

spraying SV on a control artery and calculating the ratio of intensity of SV in the different histological region to the intensity in a control area on the glass slide. Applying these ratios during the quantification allows to correct any biological matrix effect and improves accuracy of quantification.

2.3.4.2.1. MALDI Mass Spectrometry Imaging

MALDI Mass Spectrometry Imaging was performed on a 7T-SolariX (Bruker Daltonics, Bremen, Germany) equipped with a 355 nm SmartBeam II laser operated at 2000 Hz. Ionization was performed in positive ion mode using the CASI (Continuous Accumulation of Selected Ions) function of the instrument to optimize sensitivity. Mass spectrum recorded was the sum of l300 laser shots. Spectra were externally calibrated with DHB ion peaks. Spatial resolution was set at 20 µm. Imaging experiment were conducted by ftmsControl 2.2 and FlexImaging 5.0 softwares (Bruker Daltonics, Bremen, Germany). Multimaging v 1.2.6.2 software (ImaBiotech, Loos, France) was used to reconstruct simvastatine distribution and perform quantification in the different histological regions of the artery. Finally, depth profiles were obtained using Multimaging and Excel to display the concentration as a function of the distance to the lumen and thus evaluate the penetration of simvastatine in the artery wall. Process is described in the figure below.

2.3.5. Protocol validation

The seven-week period of fat diet was followed by 3 weeks of normal feeding. Before starting fat diet and one week later, a dosage of plasma cholesterol via the marginal vein of the ear was carried out After 1 week of fat diet, rabbits underwent a first surgery to create unilateral (**left**) iliac arterial injuries, the right iliac arteries were considered as a control. Pre-tracheal cervical region was shaving and disinfecting with Biseptin. In aseptic condition, an incision was made forward of the trachea in order to performing right carotid dissection. After puncture of the right internal carotid artery with needle (18 G), a 4-French introducer sheath (Radiofocus TIF TIP, TERUMO Tokyo, Japon) was inserted into the vessel, preloaded with a guide wire TERUMO 0.035’ (Radiofocus, TERUMO, Tokyo, Japon). Intravenous heparin (100 IU/kg) was then administrated via the introducer device. The left iliac artery was catheterized with a 0.018’ guide wire and a 2.75*18 mm balloon was inflated at 8 atm. Endothelial injuries were made by going back and forth with inflated balloon three times. An arteriogram (DSA) centred on the aortic bifurcation and the two iliac arteries was performed by manual injection of 5mL of Xenetic 300 (Guerbet, Villepinte, France) via a probe, before and after the balloon injuries. The right

carotid artery was ligated, the incision above the carotid artery was closed in layers, and the rabbit was allowed to emerge from anesthesia. Rabbits received then a daily intra-muscular (IM) injection of Buprenorphine 0.3ml during 3 days. Rabbits were sacrificed at the 10th week and iliac samples were harvested after a final angiography.

2.3.6. DES test

In order to test the 2 DES developped, a bi-iliac rabbit model was used, as presented figure 3B. The rabbits had an additional surgery in the 9th week. For this surgery, both iliac arteries were catheterized with a 0.018' guide wire. Each animal received 2 stents : a bare metal stent (BMS) in the right primitive iliac artery and a drug eluting stent (DES) on the left. An arteriogram (DSA) by manual injection of 5mL of Xenetic 300 (Guerbet, Villepinte, France) via a probe was performed before and after the stenting. The two femoral arteries were ligated at the end of the procedure after removal of the material and closure of the incision. Rabbits received an IM injection of Buprenorphine 0.3ml repeated daily for 3 days as the procedure progressed. The normal diet period has been extended by 3 weeks (total duration of 6 weeks). Rabbits were also sacrificed at the end of the protocol, and iliac samples were harvested and fixed in PAF after a last angiography.

2.3.7. Histological analysis

Histological analysis was performed in six hematoxylin-eosin stained cross-sections of each iliac segment (two proximal sections, two mid sections, and two distal sections), which were 5 µm (without stent) or 10 µm (with DES or BMS) thick. Measurements of the histopathologic sections were performed by using a calibrated x10 optical microscope, digital video imaging system, and microcomputer program. The slices were then analyzed using ZEN software (ZEN 2 blue version for Windows). Luminal, intimal, and medial dimensions were computed using the internal and external elastic laminae as delimeters.

The area of the neointima (NI) was determined by the difference between the area bounded by the internal elastic limit (IEL) and the area of the lumen and stent mesh. It was compared to the media by the ratio NI/media **(Figure 5)**.

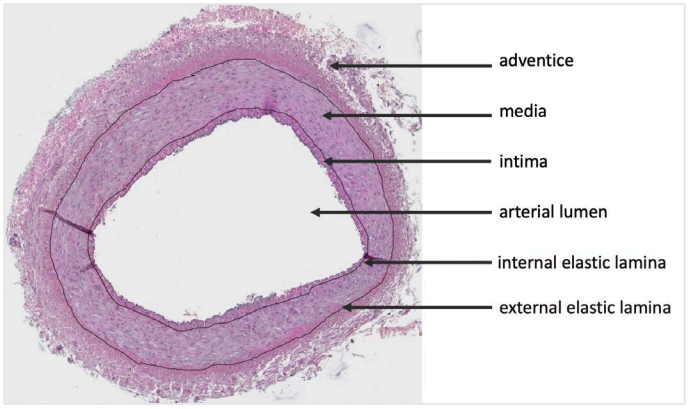

Figure 5: normal arterial section

2.3.8. Statistical analysis

The results are expressed as a mean and the associated standard deviation for quantitative values and as a % for qualitative values. Non-parametric tests, Wilcoxon and Mann and Whitney respectively, were used for comparisons of matched and unmatched means. The significance threshold was set at $p < 0.05$. IBM® SPSS® Statistics 20 software was used for the statistical tests and Excel for the graphical representations.

3. RESULTS

3.1. Preparation of NFs

Over the last 4 years, the electrospinning parameters have been optimised to obtain uniform defect-free NFs for each polymer. The morphology of the stent surface was analyzed by scanning electron microscope, as shown **figure 6**. All these membranes were obtained after 30 minutes (PCD-CHT) or 45 min (PU) of electrospinning.

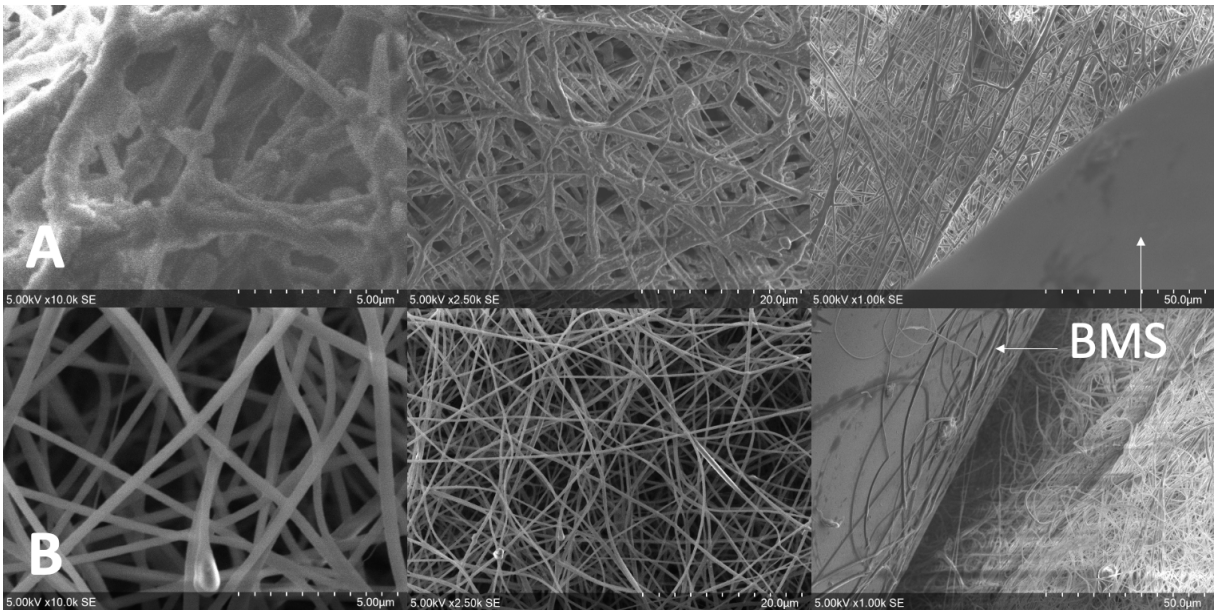

Figure 6 : Scanning electron microscopic images of drug eluting stent, (A) PU-SV eluting stent ; (B) PCD-CHT-SV eluting stent.

3.2. Cytotoxicity assay

The cytotoxicity of the different nanofibers (NFs) was evaluated according to ISO/EN 10993-5 standard by the extraction and the direct methods with Human Pulmonary Microvascular Endothelial Cells (HPMEC cells).

Figure 7 shows the cell viability results of NFs obtained by electrospinning and using the extraction method. The groups used were NFs based on hydroxypropyl β-cyclodextrin (HPβCD), polyurethane (TPU) with or without simvastatin (SV) and chitosan (CHT)/cyclodextrin polymer (PCD) containing or not SV. CHT/PCD based NFs were heat treated at 90 °C in order to remove the excess of solvent, *i.e.* acetic acid and subsequently rinsed 10 seconds in a 4g/L sodium bicarbonate ($NaHCO_3$) solution and 10 seconds in a of 0.9 % saline (NaCl) solution to neutralize any excess of acetic acid remaining left within the NFs.

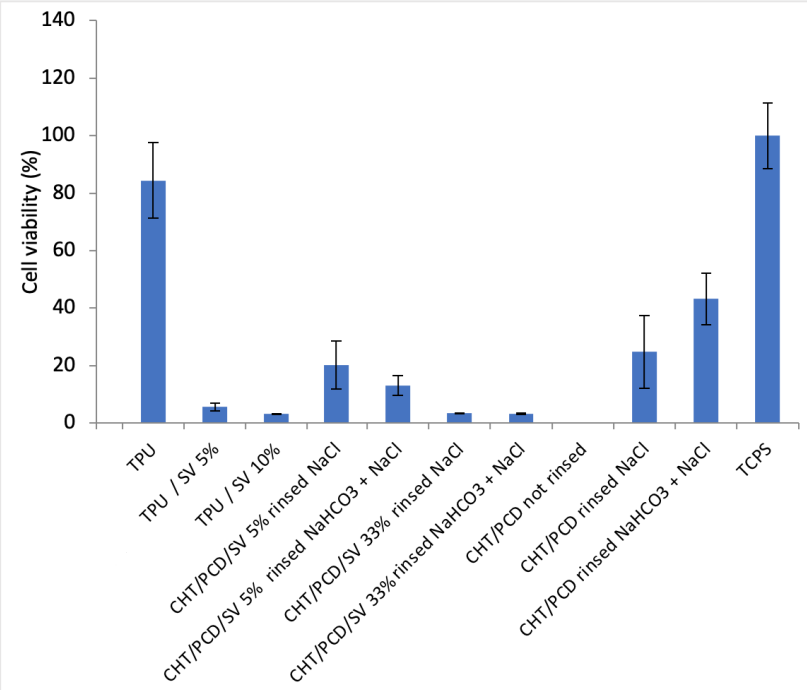

Figure 7: Cell viability rate of HPMEC cells on nanofibers obtained by electrospinning using the extraction method.

All the NFs containing SV exhibited very low cell viability, *i.e.* < 30 %. Moreover, the cytotoxicity of NFs increased by increasing the concentration of SV, for example the cell viability was reduced from 20.21 to 3.36 % with 5 and 33 % of SV, respectively, for CHT/PCD NFs. The cell viability of TPU NFs with 0 and 5% SV was reduced from 84.38 to 5.66 %, respectively. In general, CHT/PCD NFs without SV were less cytotoxic, with a mean cell viability of 55 %. These results confirmed the cytotoxic effect of SV on cells. Unfortunately, the cell viability results on NFs without SV and rinsed with the NaCl solution still not sufficient as this was inferior to 70 % of cell viability. Hence, CHT/PCD NFs still have to be fine-tuned to be less cytotoxic.

In order to improve their stability, CHT-based NFs were heat treated at 120 °C for 4 h. This treatment created the formation of hydrogen bonds. Different rinsing times with $NaHCO_3$ and NaCl solutions were studied. **Figure 8** displays the cell viability results for CHT/PCD NFS rinsed with $NaHCO_3$ and /or NaCl for different times. The results revealed that rinsing NFs with NaCl increased their cytocompatibility. No cell viability has been observed for nanofibers treated at 140 °C for 4 h and not rinsed, while NFs rinsed for 5 minutes in NaCl exhibited a cell viability of 89 %. All samples rinsed with NaCl and/or $NaHCO_3$ were not cytotoxic, *i.e.* cell viability superior to 70 %. This enhancement of cytocompatibility

can be explained by the fact that washing NFs removed the excess of solvent, *i.e.* acetic acid, remaining even after the heat treatment. In conclusion, washing nanofibers 5 minutes with NaCl improved the cell viability.

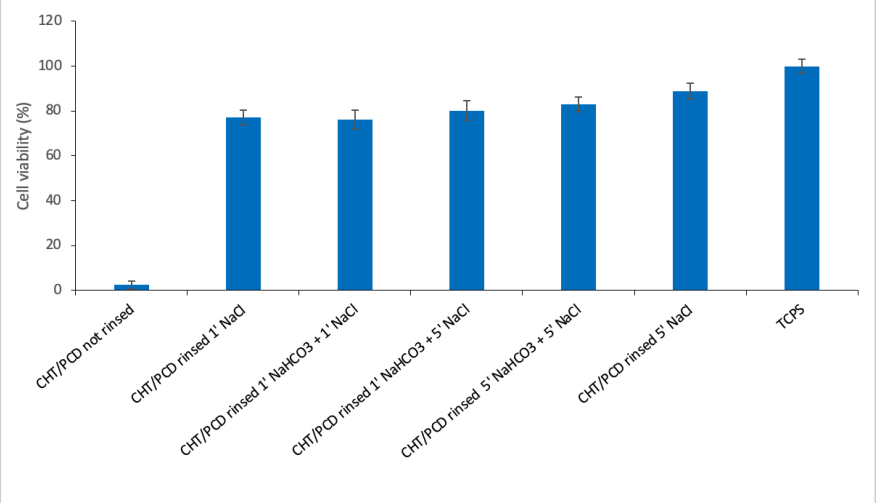

Figure 8 : Cell viability rate of HPMEC cells on CHT and PCD nanofibers without SV

3.3. Cytocompatibility assay

The cytocompatibility assay was also done by using the direct contact method to evaluate the cell viability of cells in contact with NFs. Figure 3 shows the results using CHT/PCD NFs heat treated at 120 °C for 4 h and subsequently rinsed with $NaHCO_3$ or NaCl solutions. The results showed that cell viability was the higher, but still inferior to 70%, for NFs rinsed with NaCl for 5 min when using the direct contact method. This lower-than-70 % cytocompatibility can be explained by the surface roughness of the samples which could not be favorable to cell proliferation *in vitro*. Other studies will be performed by using atomic force microscope (AFM) in order to elucidate the effect the roughness, and the elasticity, of the surfaces obtained by the different CHT/PCD may have on cells while being in direct contact with the different substrates. For the TPU cell viability was of 79 % while using the direct contact method.

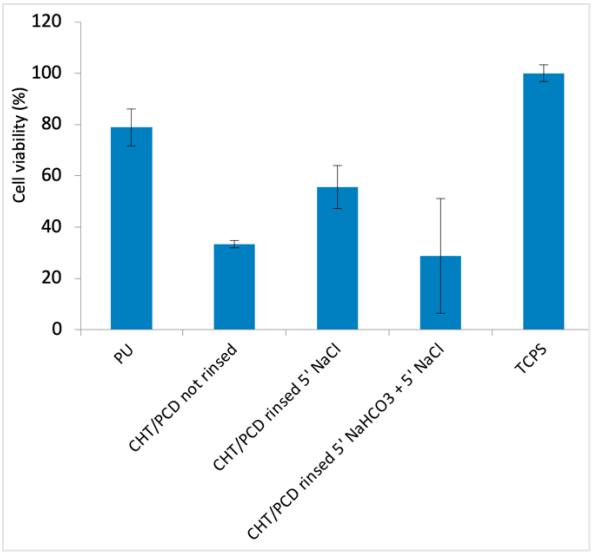

Figure 9: Cell viability rate of HPMEC cells using direct contact method.

3.4. Drug release

Due to the targeted antirestenosis application, it is necessary to determine if the amount of simvastatin charged on NFs is sufficient to achieve therapeutic activity. In the literature, it has been suggested that the therapeutic quantity of rosuvastatin (another type of statin) loaded nanofibers is comprised between 2 and 5 µg/mm^2.

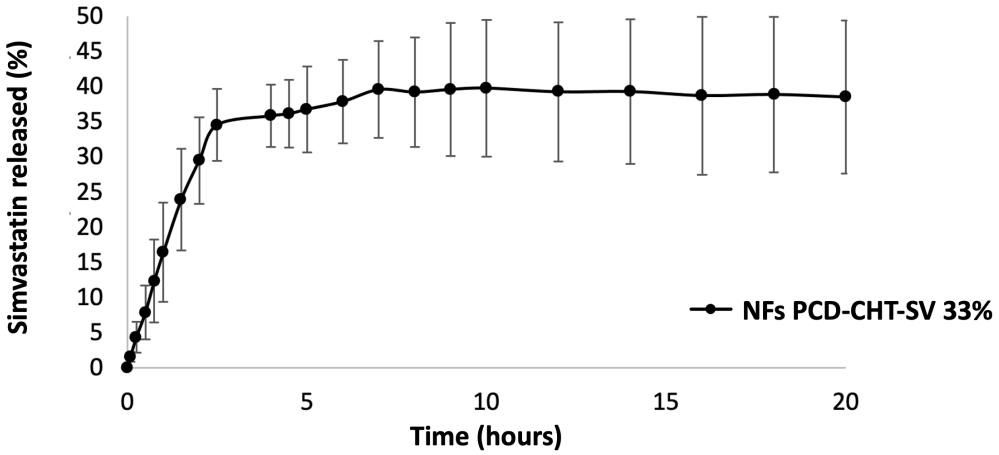

Figure 10 : in vitro release kinetics of PCD-CHT-SV eluting stent

Previous work in the U1008 laboratory investigated the release profiles of stentless electrospun membranes, including the influence of the duration of electrospinning, the percentage of PCD in the nanofibers and the quantity of simvastatin (5 to 33%).

The following experiments were used to define the release profile of electrospun stents. They have been investigated under the same conditions, i.e using a dynamic system (35 mL/min) at 37 °C in PBS (pH 7.4) containing 0.7% w/v of SDS. The addition of SDS was necessary in the release study to increase the solubility of SV. The aim was to determine if the therapeutic quantity of SV released has been reached.

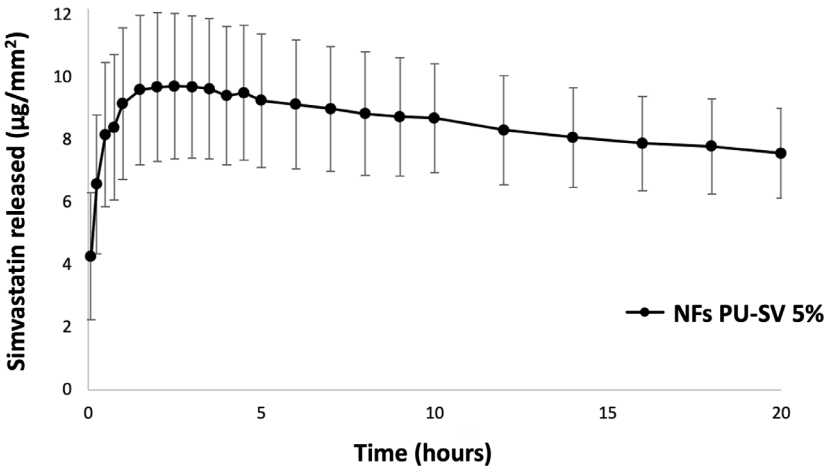

Figure 11 : in vitro release kinetics of PU-SV eluting stent

Figure 10 and 11 display the kinetic release profiles of SV of nanofibers made of PCHT-CHT or PU and charged with respectively 33% (w/v) or 5% (w/v) SV. The results are expressed as a percentage (**figure 10**) and as quantities in µg/mm^2 (**figure 11**). These profiles are close to those obtained on membrane alone. The release of SV in NFs PCD-CHT seems to be slower than nanofibers made of PU. It is difficult to explain the trend in the release profile of PU stents. Investigations are still ongoing.

3.1. In vivo study

Four sets of rabbits were required : one set for the pharmacokinetic study, a second for the validation of the animal model and two sets for DES assays, i.e. a total of 41 rabbits.

3.4.1. In vivo pharmacokinetic study (Fig. 10)

3.4.1.1. Biological sample preparation

9 rabbits were received an aortic stent : 1 BMS, 7 PCD-CHT-SV stents and 1 PU-SV stent.

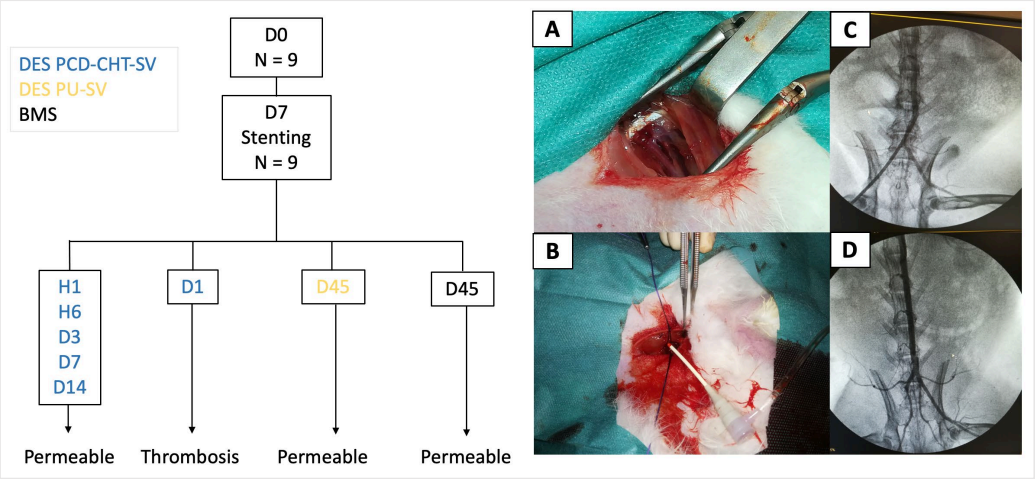

Figure 12: Stenting of the subrenal aorta, (A) dissection of the right femoral artery, (B) 5F introducer in the femoral artery, pre (C) and post (D) stenting arteriography.

One rabbit was sacrificed on the first day because of a sub-renal aorta thrombosis due to arteria dissection during the setting up of the introducer sheath. The other stents retained potency on final arteriography (**figure 13**). Because of the COVID-19, the rabbits were sacrificed at D45.

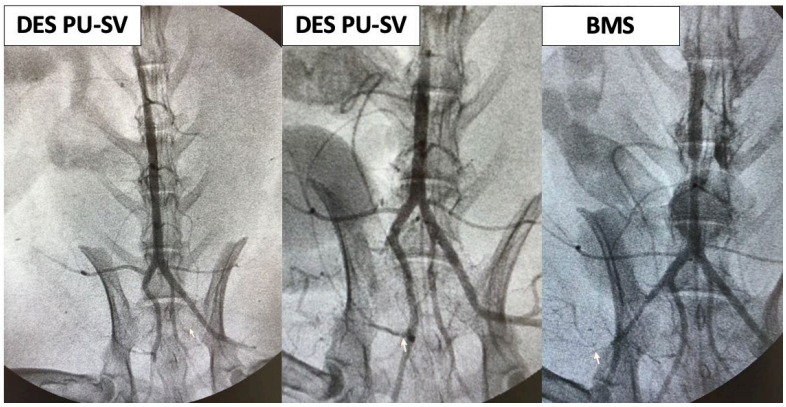

Figure 13: final arteriography before sacrifice on the 45th day

3.4.1.2. MALDI Mass Spectrometry Imaging - standards

Simvastative was detected in standard as sodium adduct [M+Na]+ at *m/z* 441.2596 (**Figure 14**). No interfering peak has been detected at the *m/z* of the drug, hence validating the specificity of the analytical technique.

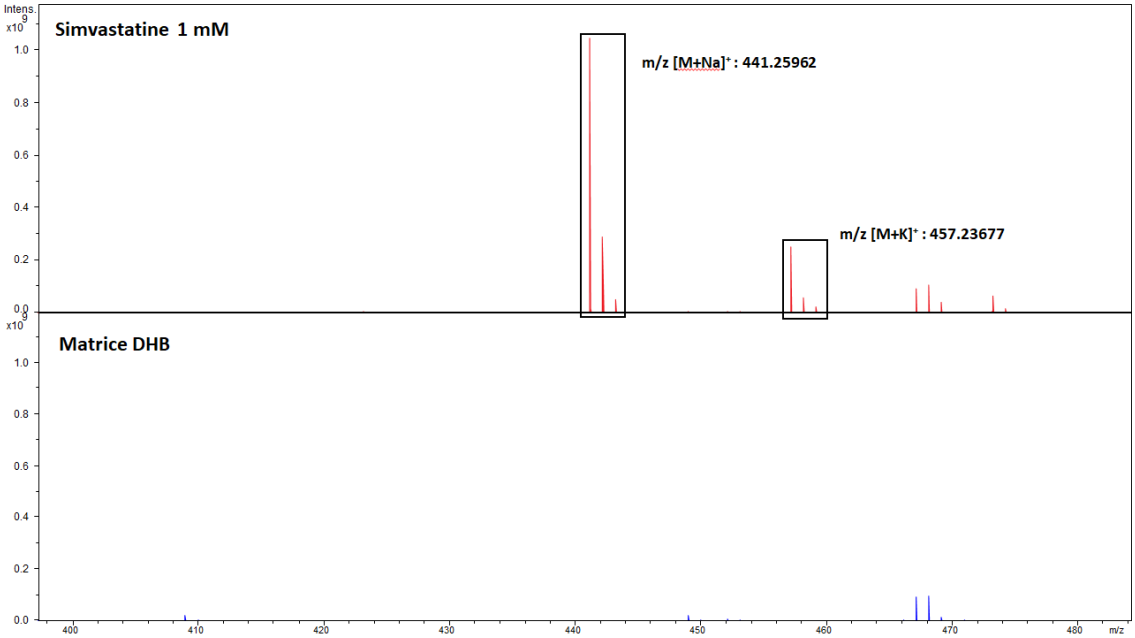

Figure 14: Mass spectrum of a simvastatine standard showing sodium and potassium adducts. NO interfering peak from the matrix was observed.

Calibration curves built with Multimaging software are presented in **Figure 15** and characteristic parameters in **Table 1**. Lower Limit of Quantification (LLOQ) was determined at 0.481 µg/g which is a very satisfying analytical performance for MALDI MSI.

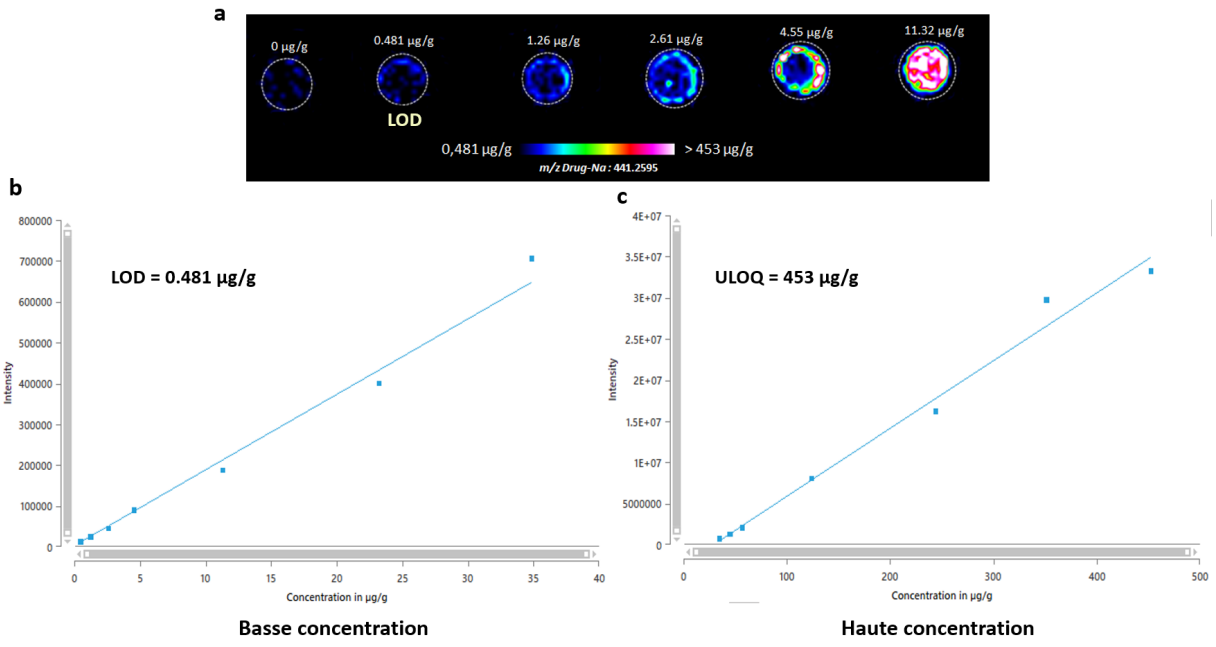

Figure 15: Molecular image of a dilution range and the associated calibration curves in the low and high ranges.

Table 1: Quantification parameters for simvastatin by Quantitative MSI

Calibration range	Concentration (pmol, Spotted on tissue)	Concentration (µg/g of tissue)	R^2	LOD (µg/g)	ULOQ (µg/g)
Low	0.1 - 7	0.481 - 34.9	0.991	0.481	34.9
High	7 - 100	34.9 - 453	0.991	34.9	453

3.4.1.1. Biodistribution of simvastatin in rabbit arteries by MALDI MSI

For each time point of the PK experiment, one molecular image has been obtained, showing the biodistribution of SV in tissue. Molecular images are presented in **Figure 16** and **Figure 17**.

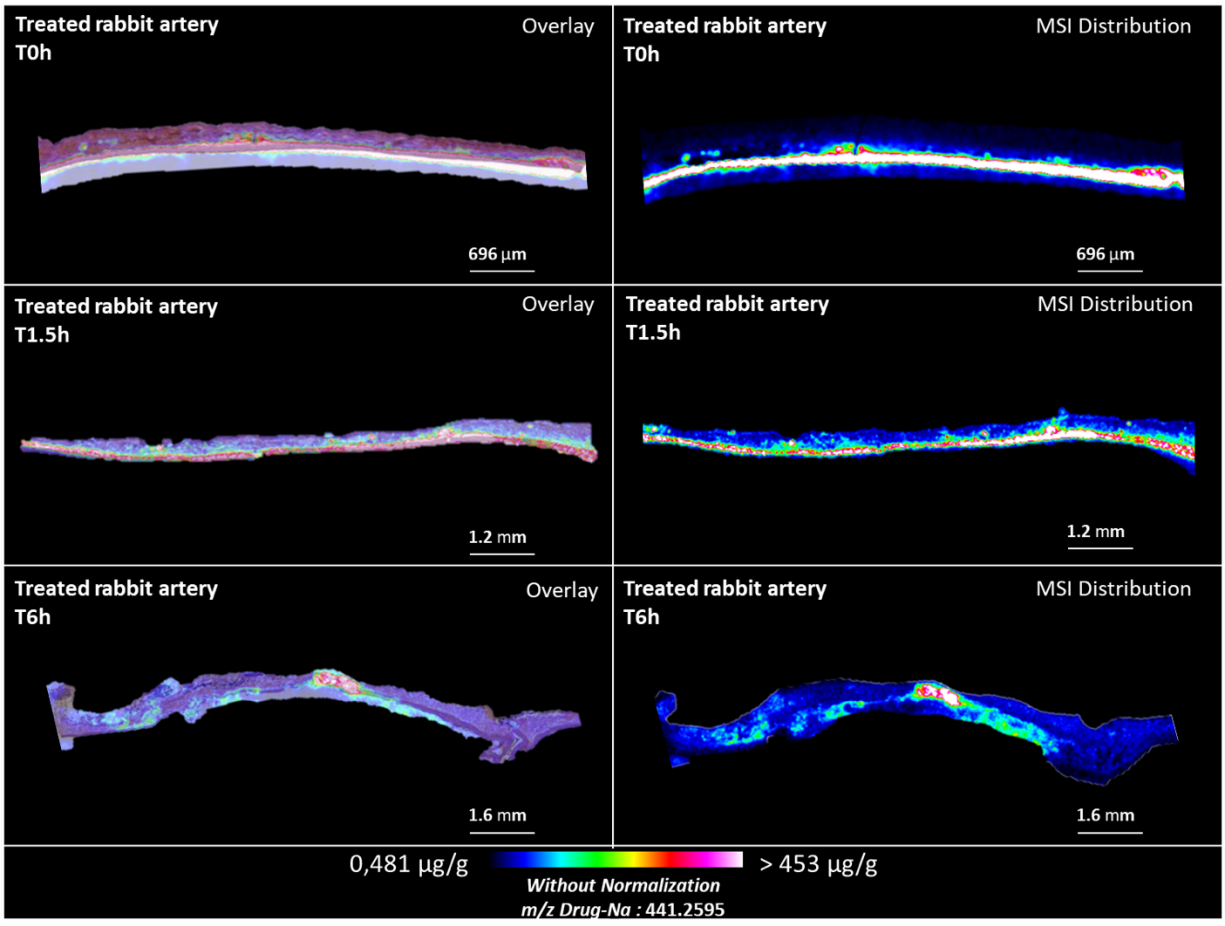

Figure 16: Molecular images of SV and overlay with H&E-stained sections for rabbit arteries collected at 0, 1.5 and 6h

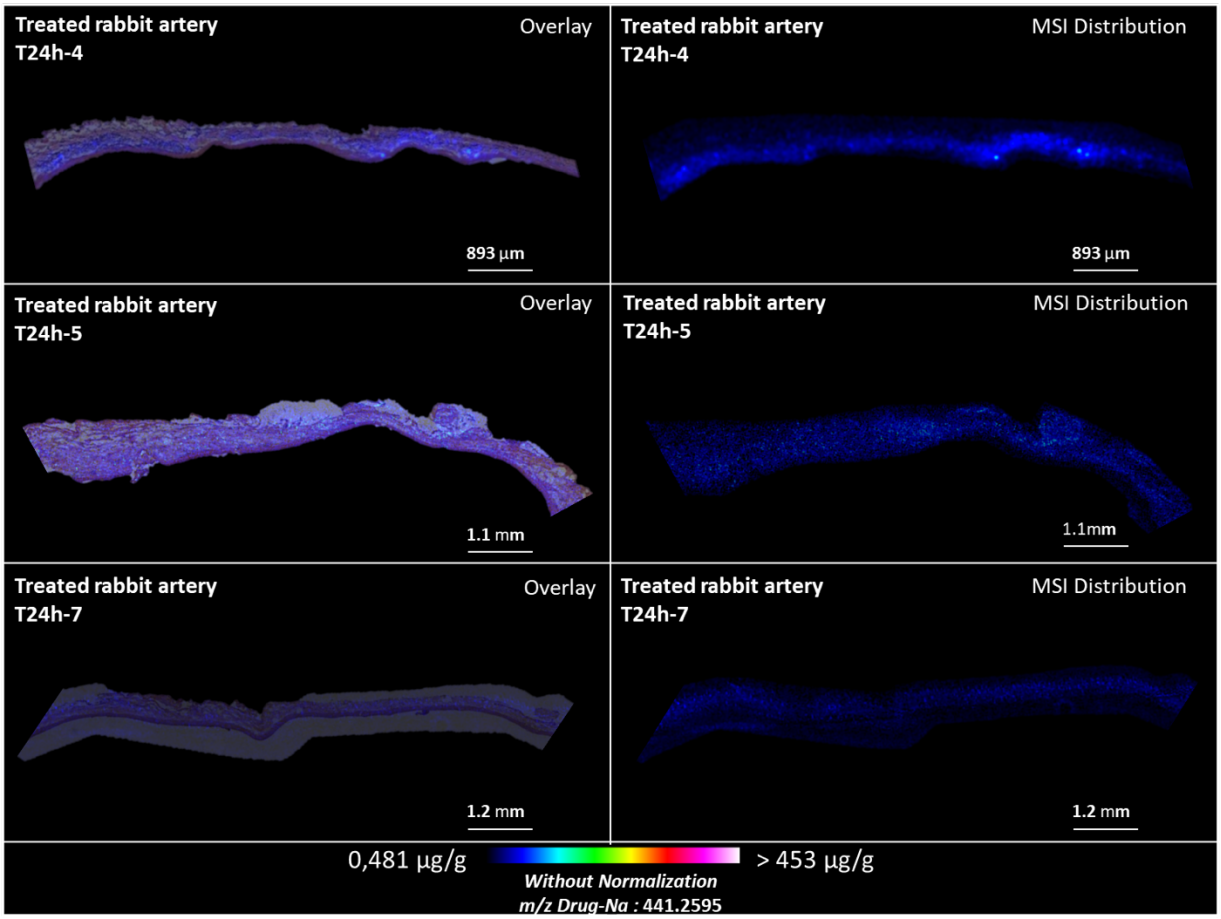

Figure 17: Molecular images of SV and overlay with H&E-stained sections for rabbit arteries collected at 24h

Interpretation has been done by correlating molecular images with H&E-stained images in order to associate concentrations of SV with each histological region (intima, media, adventice). As stent removal has damaged the intima, the histological region in contact with the stent, the analysis had to focus on media and adventice.

Molecular images showed qualitatively the biodistribution of SV in both histological regions. Deep penetration of SV has been obtained since a higher intensity of SV signal is observed in the adventice.

Delineation of intima and adventice has been done for each sample in order to quantify SV in these histological regions and build penetration profiles. Below are examples of penetration profiles of SV obtained at 0h (**Figure 18**) and 24h (**Figure 19**) showing rapid distribution of SV in the different layers of the artery wall, with highest concentrations observed in the adventice.

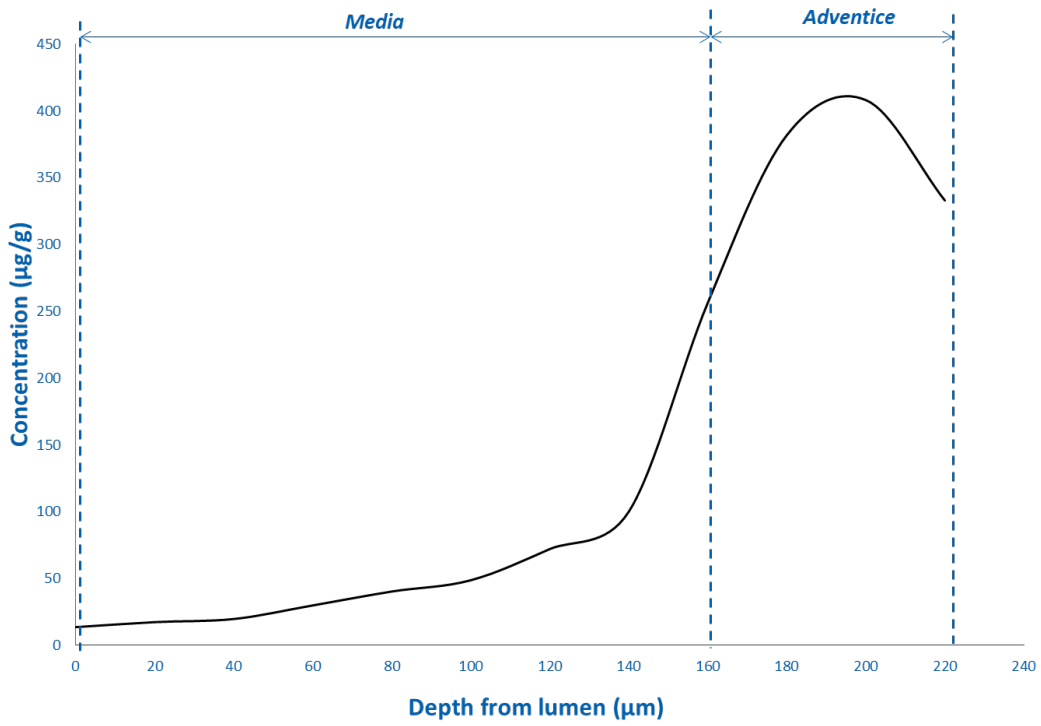

Figure 18: Penetration profile of SV in rabbit artery wall at 0h

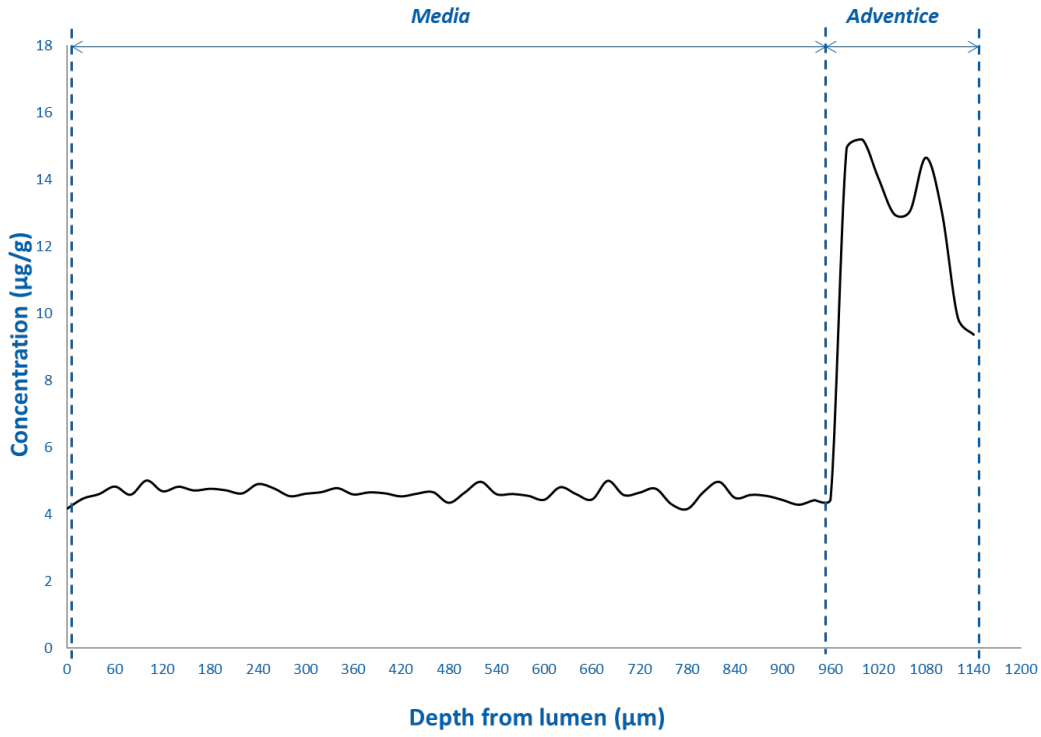

Figure 19: Penetration profile of SV in rabbit artery wall at 24h

Figure 20 presents the overlay of all penetration profiles obtained in the tissue PK study. Differences in tissue thickness explained the differences in x-axis on the graph. Despite these differences, a consistent trend for higher concentrations of SV in adventice is observed for all samples.

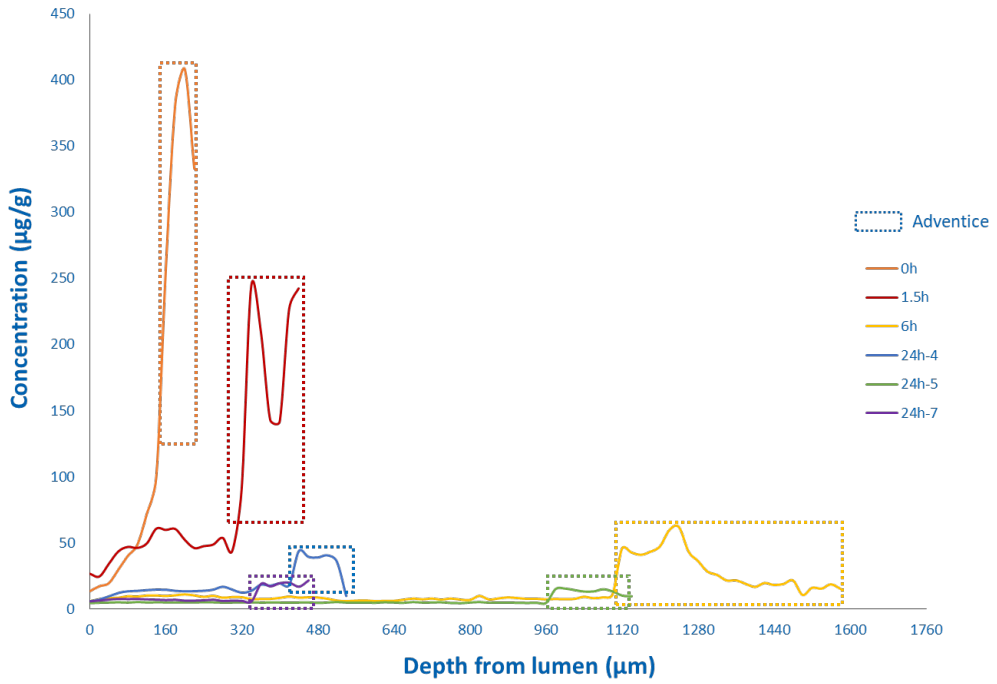

Figure 20: Overlay of all penetration profiles of SV in rabbit artery walls

Concentration – time profiles have been finally plotted for both media and adventice and are presented in **Figure 21**. The graph confirms the consistently higher concentrations of SV in adventice, whatever the time point considered. Media is indeed 5 times less exposed to SV than the adventice, based on AUC calculations. Tmax is 1.5h for both histological regions. Associated Cmax is 350 µg/g and is observed in adventice. Half-life of 10h has finally been determined for both media and adventice.

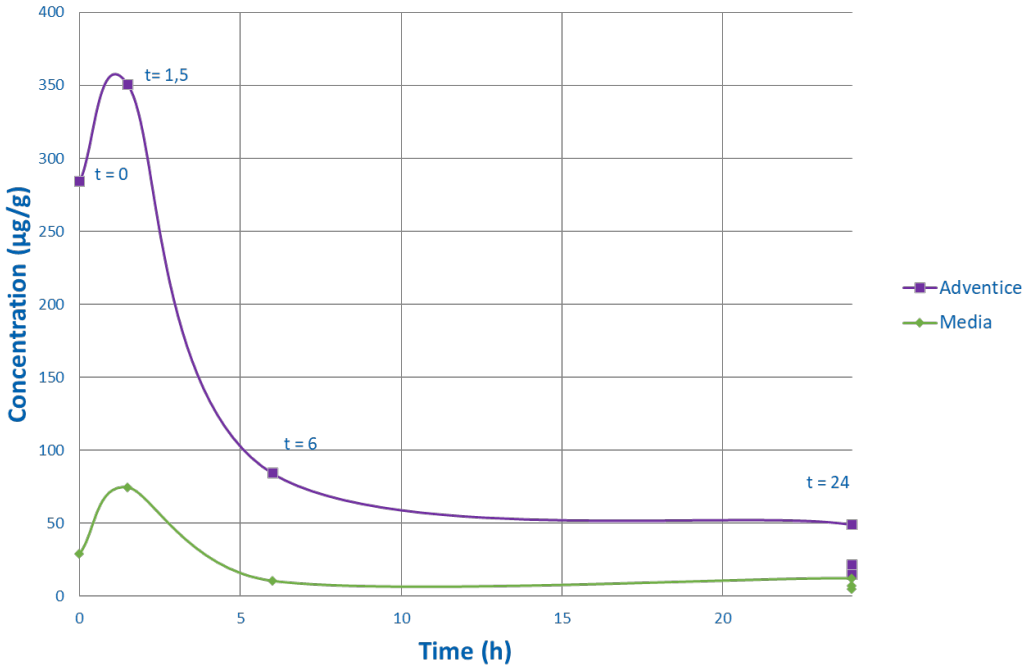

Figure 21 : Concentration – Time profile of SV in media and adventice

3.4.2. Protocol validation

Among 12 rabbits, only 8 survived to the end of the protocol. Causes of death are presented in the flow chart in **Figure 22**. Final angiography before sacrifice revealed more than 50% iliac stenosis in 4 of the 8 injured arteries.

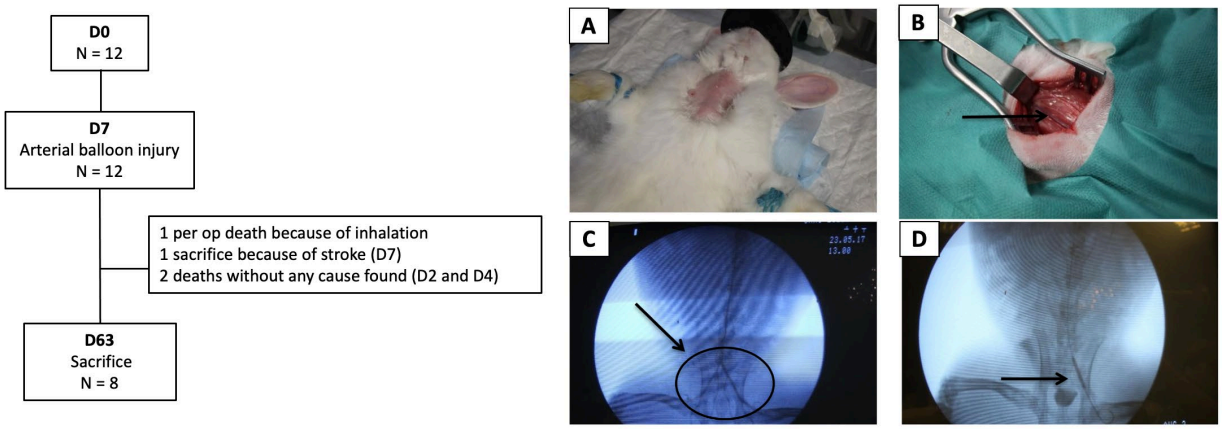

Figure 22: Flowchart of rabbit for atherosclerosis formation ; installation and pre-tracheal shaving (A), dissection of the right carotid artery (B), iliac arteriography (C) and iliac arterial balloon injury (D).

Histological analysis showed **Figure 23** a significative difference in the ratio neointima/media between left iliac (with arterial balloon injuries) and right iliac (without arterial balloon injuries).

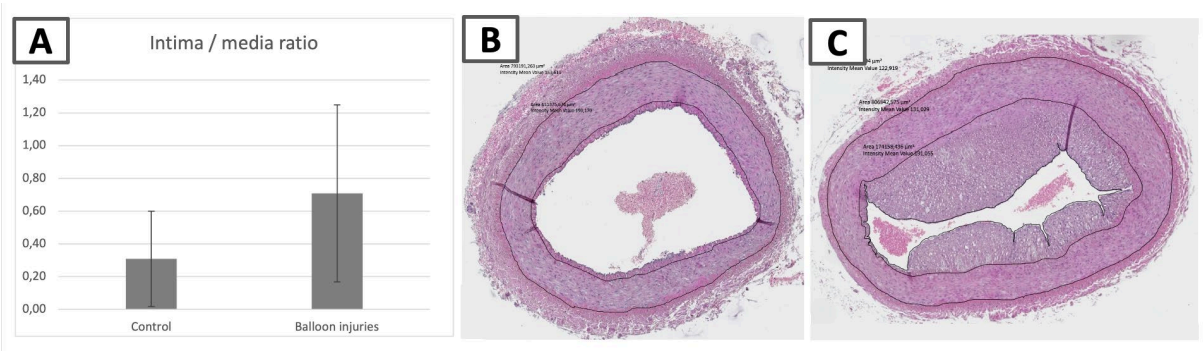

Figure 23: ratio neointima/media (A), right iliac artery section without arterial balloon injuries (B) and left iliac artery (C).

3.4.3. DES candidates

This rabbit atherosclerosis model was developed in order to test both DES elaborated in the laboratory INSERM U1008 and UMET. In order to evaluate the PCD-CHT-SV and PU-SV DES, 8 and 12 rabbits have been respectively involved and only 7 rabbits completed each protocol **(Figure 24).**

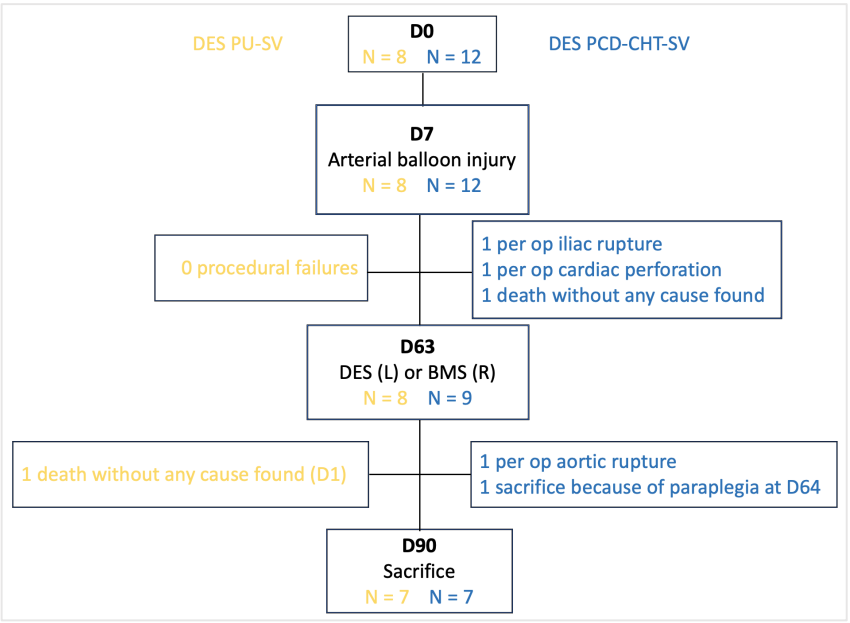

Figure 24: flowchart for PU-SV and PCD-CHT-SV stents in vivo analysis.

The final angiography before stenting revealed more than 50% iliac stenosis in 5 of the 18 injured arteries in the PCD-CHT-SV and the PU-SV group. The final arteriography achieved at the 13th week

showed a high thrombosis rate for PCD-CHT-SV and no significative difference for the PU-SV stent for the neointima/media ratio (**Figure 25**).

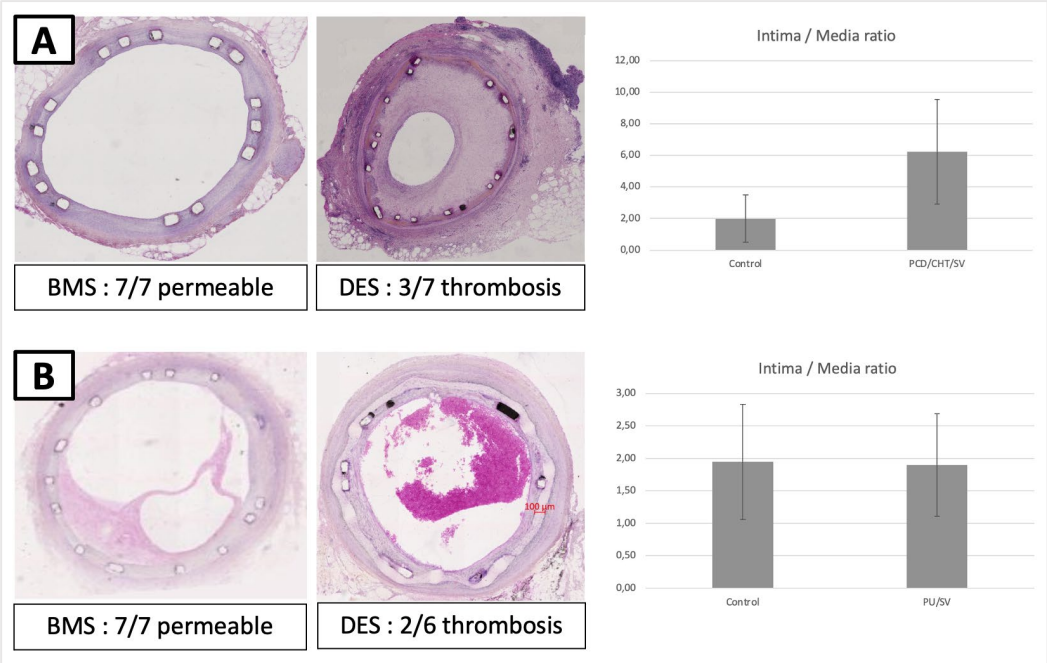

Figure 25: In vivo study results for PCD-CHT-SV (A) stent and PU-SV stent (B).

These results are not conclusive for the stent made of PCD-CHT-SV but suggest the interest of further explorations of the stent PU-SV.

3.5. Polymer characterization and HME optimization

Prior to extrusion processing the plain polymers and their blends were physiochemically characterized using Differential Scanning Calorimetry (DSC) and Thermogravimetric analysis to investigate their thermal stability and hence the extrusion temperatures. Blend miscibility could also be analysed via determination of thermal events of blended polymers in comparison to the pure specimens. The DSC thermographs in Fig. 26 show that for Resomer L206S there is an endothermic transition, typical of a melting point, at 186.05°C. The highly crystalline polymer, Resomer X206S, displayed a melting point peak at 111.60°C while the amorphous, Resomer R205S, displayed a glass transition temperature at 55.58°C. It was observed that in the second cycle of heating for the pure polymers that the temperature of their transition decreased very slightly. This depreciation of temperature of transition is common and indicates that the materials have become slightly more amorphous due to having been heated once already.

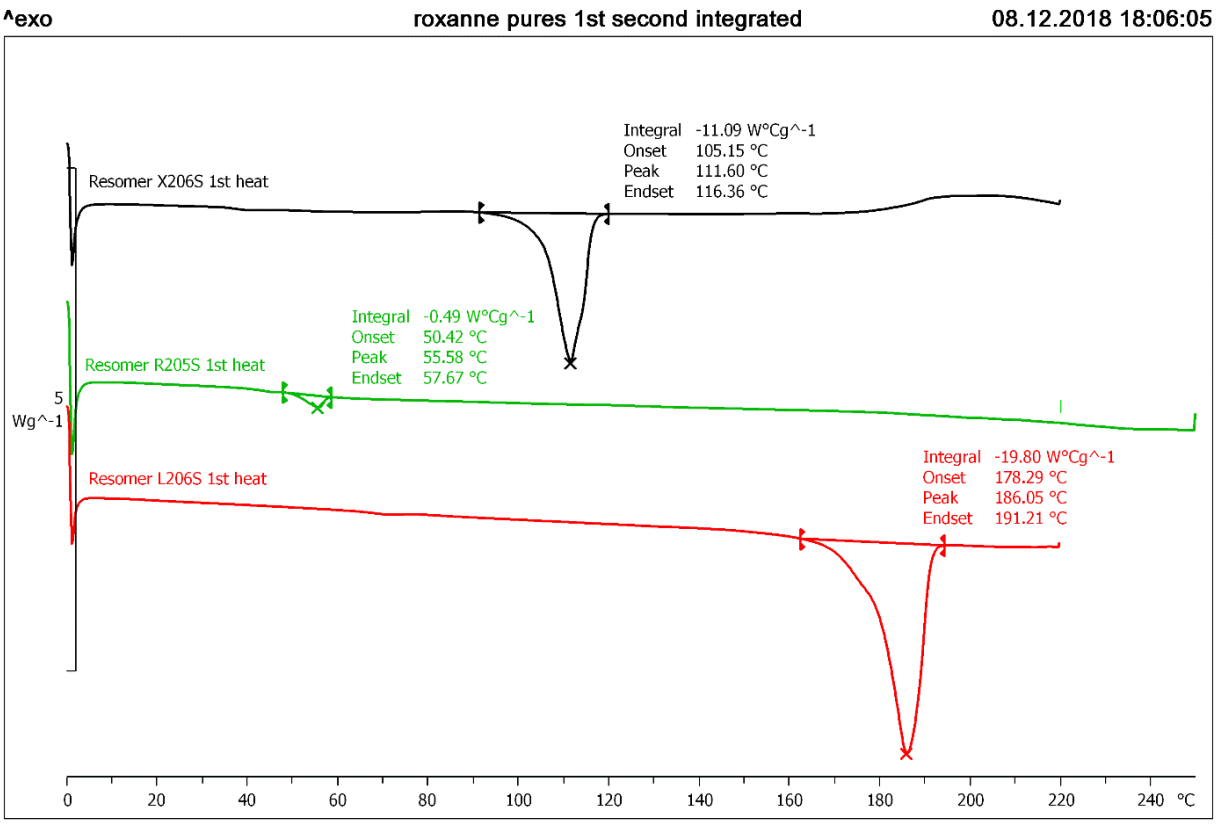

Figure 26: DSC thermographs of the bulk polymers

The thermal behavior of polymer X206S was investigated further by running a separate analysis (thermogram not shown). The thermographs from the 1st and 2nd heat it was apparent that there is a depreciation in the melting point, from 110.93°C in the first heat of the sample to 105.26°C in the second heat of the sample, indicating that the sample has not transformed totally back into its original more crystalline structure but has rather increased its amorphicity over the cooling stages. Also, it can be seen that there is a glass transition from -11.85°C to -9.37°C occurring in the second heat, this glass transition is not present in the first heat so is confirmation of increased amorphicity in the sample after the first heating stage. This glass transition is the transition from rubbery to glassy amorphous state.

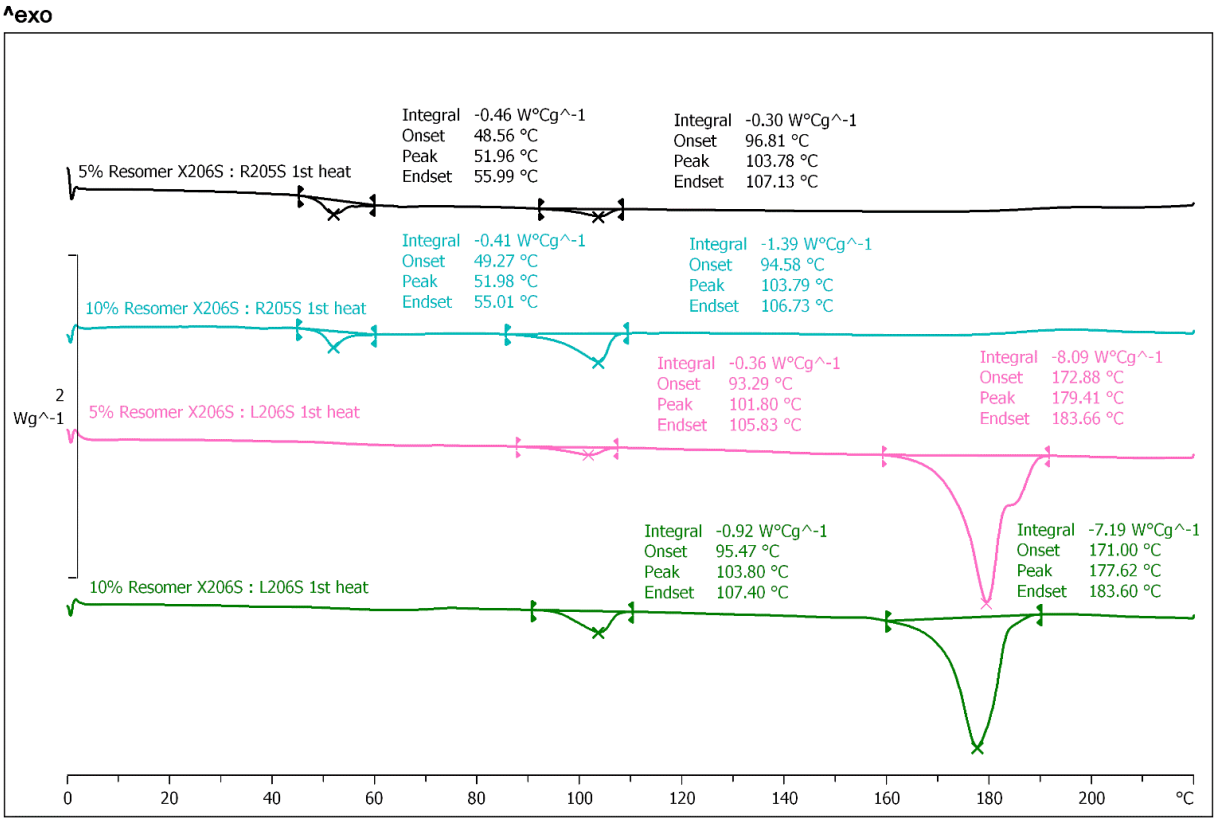

Figure 27: DSC thermographs for the two polymer blends in 5% and 10% ratios

DSC thermographs shown in Fig. 27 show the 5% and 10% blends of Resomer X206S with either Resomer R205S (black and teal lines respectively) or Resomer L206S (pink and green lines respectively). As expected, the blends with 5% X206S show shallower peaks as compared to 10% blends at the polymer's melting point at 103.79°C. This is confirmed by the enthalpy of the constituent polymer being decreased in comparison to the increasing amount of Resomer X206S. This indicates that the blends with higher percentage of Resomer X206S have a larger change in enthalpy as compared to the 5% blend which is expected when there is a larger amount of the material present. Two distinct thermal events can be observed in each blend that correspond with the temperature of phase transition in the respective pure polymer.

Observation of two distinct thermal events is an indicator that the two materials may not be miscible. However, the depression in melting point of Resomer X206S from 111.60°C to 103.79°C (Fig. 17) is an indication that there is a more complex interaction between the two polymers, leading to a decrease in melting point. Studies of melting point depression have been used to assess interaction between different polymer segments. In blends with stronger interactions, the melting point depression is larger

and can be 5-10°C or more. In Fig. 15 a large decrease in temperature of melting point of approximately 8°C is seen in Resomer X206S melting point peak present in all the blends. Resomer R205S when blended with X206S, experienced a decrease in its melting point peak to 51.96°C in the 5% blend and 51.98°C in the 10% blend. Resomer L206S when blended with X206S shows a decrease in temperature of its melting point to 179.41°C and 177.62°C in the 5% and 10% blends respectively.

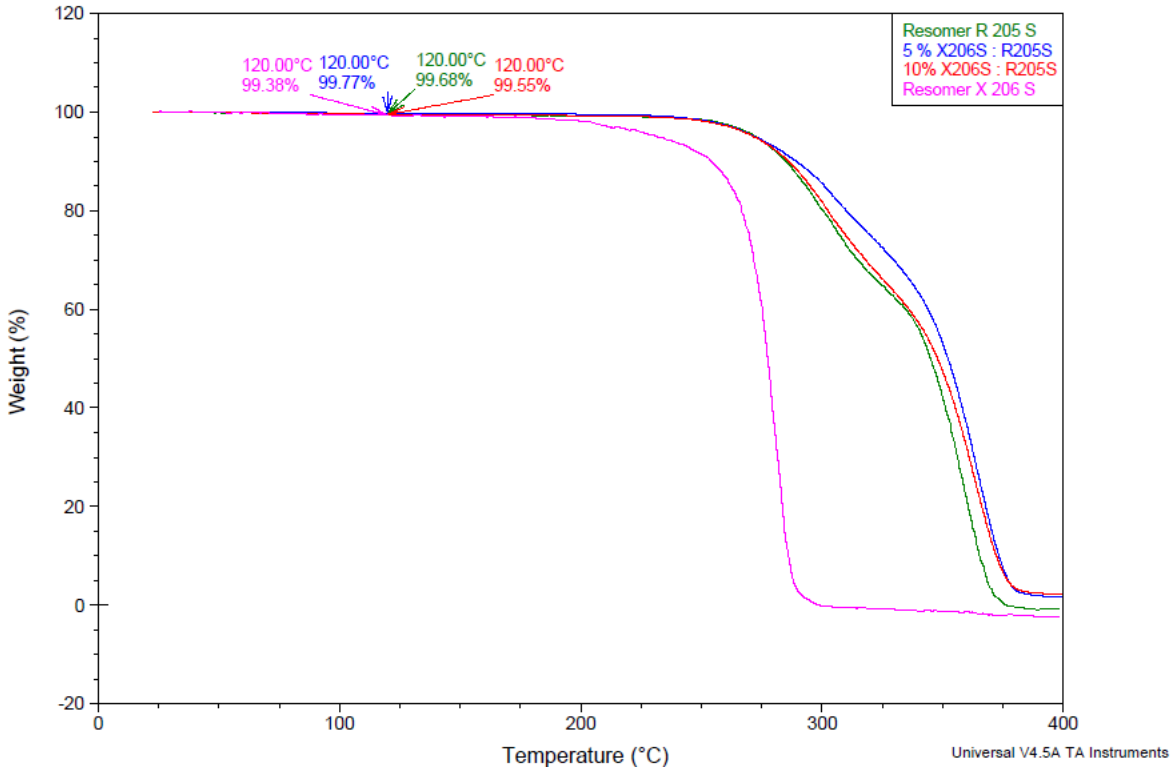

Figure 28: TGA plot for Resomer R205S, Resomer X206S and their blends. Showing percentage mass loss at processing temperature of 120°C.

The degradation/ decomposition temperature was identified for each bulk polymer and polymer blend using dynamic heating rate TGA. Gaining knowledge on the behaviour of the polymers under high temperature condition, alone and in combination is important because during the printing process the polymers will need to be subjected to high enough temperatures for their extrusion. For application as a 3D printing material, the suitable polymers would be ones which do not undergo weight loss below the temperature at which they are to be processed at. This is to ensure integrity of the material and stability of the mechanical properties of the material. Thermal stability measured by TGA can give good indication to material suitability for the application.

Fig. 28 shows the degradation profile Resomer X206S and its blends with R205S. It can be seen that at the processing temperature of 120°C no sample loss occurs. The fastest rate of degradation onset occurs where the linear portion of the curve is steepest indicating the mass loss percentage at this point is the greatest. However, at the temperatures used for the material's processing there is no mass loss occurrence associated with degradation. The TGA profiles of the pure polymers and 5% and 10% blends of Resomer X206S with Resomer L206S (Fig. 29) show that degradation onset is also at a much higher temperature than the current processing temperature. Only a minimal loss of mass of approximately 1% occurs at the processing temperature 190°C for the blends of Resomer X206S with Resomer L206S.

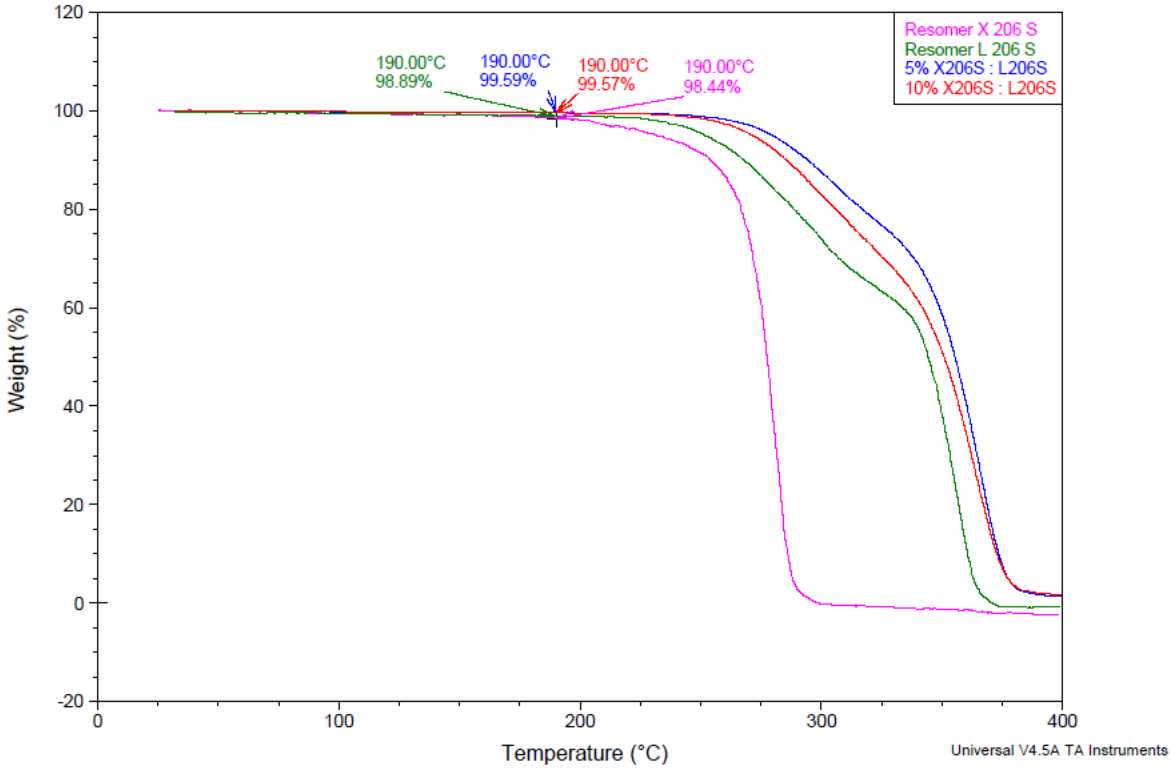

Figure 29: TGA plot for Resomer L206S, Resomer X206S and their blends. Showing percentage mass loss at processing temperature of 190°C.

The lowest and highest temperature of degradation when comparing all the blended materials is 325°C and 335°C respectively, this is the point where 99% of mass of sample is lost. The degradation point of the blends has shifted to a higher temperature because of the molecular interactions between its constituents.

Based on the above results the HME processing was optimized by adjusting the feed rate of powder blends, screw speed and temperature profile. A shown in Fig. 30 (B, C) the SEM analysis of extruded filaments showed a smooth surface with no defects. Subsequently, the filaments were collected on the cartridge (Fig. 30D) prior to stent printing. As shown in Fig. 20A the extruded filaments are directed to a 3D printing line and collected on the cartridge. The thickness uniformity is controlled by a laser gauge which measured continuously the obtained filament width and by feeding the information it can control the rate of the rollers in the 3D line. The 3D line can control accurately the desired width of the filament facilitating uniformity across the production process and smooth printing of the designed structures.

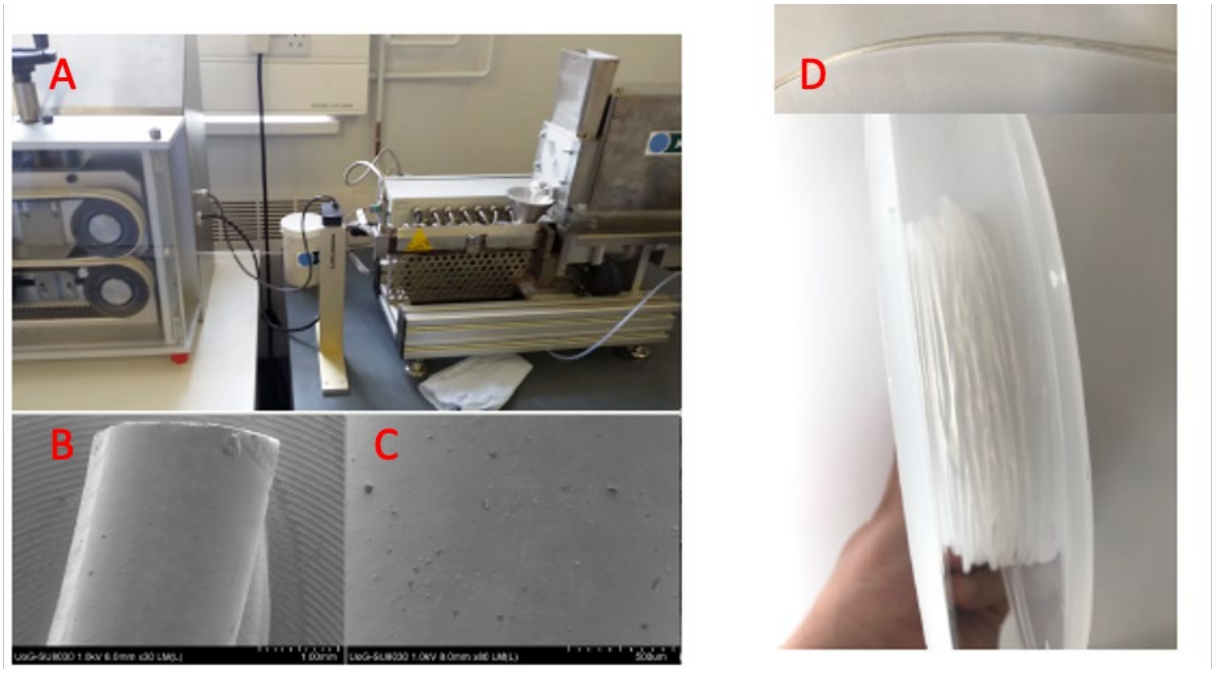

Figure 30: SEM and optical images of extruded polymers for the fabrication of printable filaments.

Bioabsorbable polymeric filaments were fabricate by hot melt extrusion (10mm extruder, Rondol, France) by optimizing extrusion speed, feed rate and temperature profile **(Figure 31A**). Mechanical property data from the tensile tests were generate using a Texture Analyser (**Figure 31B),** Stable Micro Systems Ltd., UK) and expressed in the form of Force (N) and displacement (mm) Subsequently, from the obtained values, engineering stress (σ) and engineering strain (ε) were plotted.

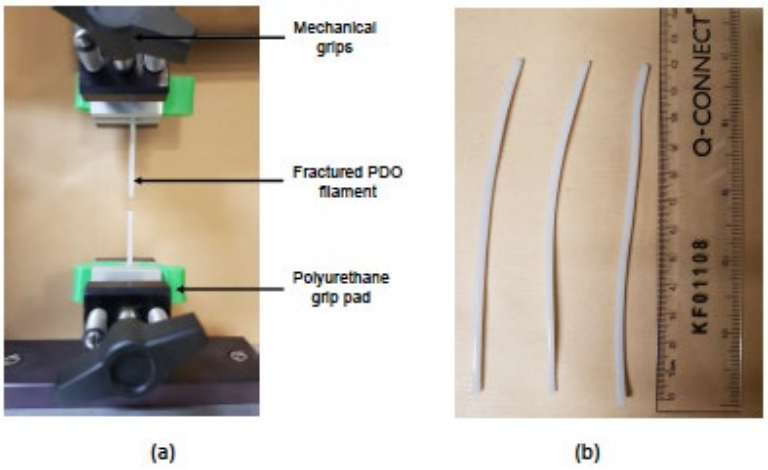

Fig. 31: A) Hot Melt Extruded filaments of polydioxanone (Resomer X206S) and b) Uniaxial testing of polydioxanone showing gripping system with fractured test specimen.

Stress was calculated as:

$$\sigma = \frac{F}{A_0} \quad (1) \qquad \varepsilon = \frac{l_i - l_0}{l_0} \quad (2)$$

Where F= force applied perpendicular to cross-section of the sample and A0 is the original cross-sectional area of the sample. Strain was calculated from (2) where l_0 is the length of the sample before force is applied (before loading), and *l*i is the sample length at any point during test.

Hooke's law states that stress and strain are directly proportional within the linear portion (elastic limit) of a stress-strain graph:

$$\sigma = E\varepsilon \quad (3) \qquad E = \frac{\Delta\sigma}{\Delta\varepsilon} \quad (4)$$

E is the modulus of elasticity (Young's modulus) (MPa) therefore calculation of the gradient of this portion of the stress-strain curve gives the value for E. Within the elastic region, the ratio of the change in stress (Δσ) to change in strain (Δε) gives value for Young's modulus, *E*.

In calculating the nominal stress–strain response of a material, it is assumed that the cross-sectional area of a tensile sample is constant over the duration of the deformation and this results in an engineering stress-strain diagram. However, for samples that experience significant stretching (deformation) beyond its elastic and yield regions, the cross-sectional area of the specimen changes significantly with deformation. Therefore, it is important to derive the true stress-strain graph, by accounting for the effect of changing cross-sectional area during the finite deformation. This true

stress-strain graph gives, especially for polymers, a representative view of the actual/intrinsic behaviour of the material. The true stress-strain data is calculated from the experimentally-determined nominal stress-strain data by using the following equations:

$$\text{True Stress:} \quad \sigma_T = \sigma_N (1+\varepsilon_N) \tag{5}$$

$$\text{True Strain:} \quad \varepsilon_T = \ln (1+\varepsilon_N) \tag{6}$$

Fig.32A shows the difference between the true and nominal stress-strain for X206S polymeric material. One can readily observe that X206S has an actual ultimate tensile strength (UTS_{true} = 28 MPa) higher than the nominal value ($UTS_{nominal}$ = 23 MPa).

A

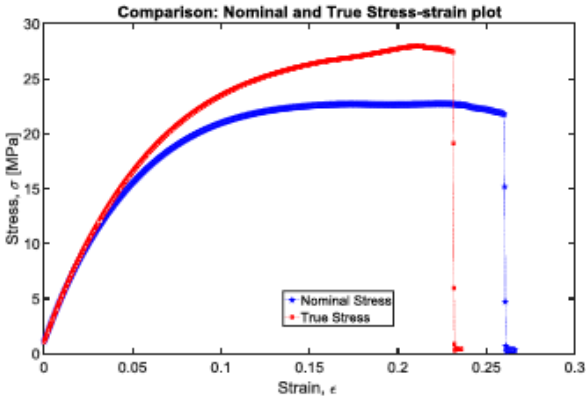

B

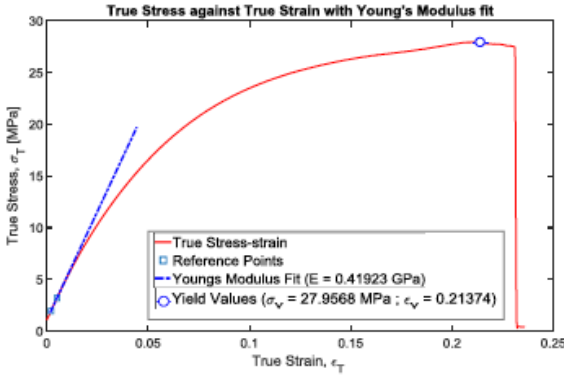

C

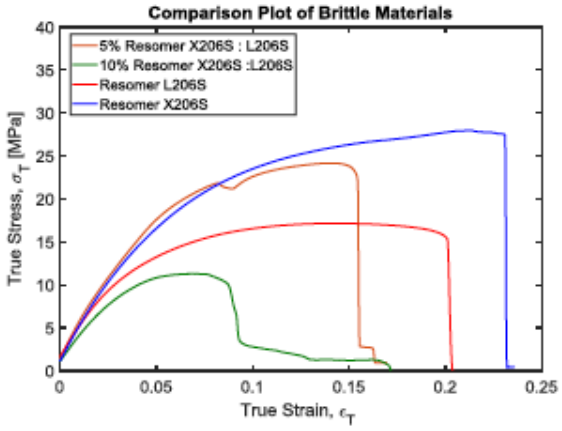

D

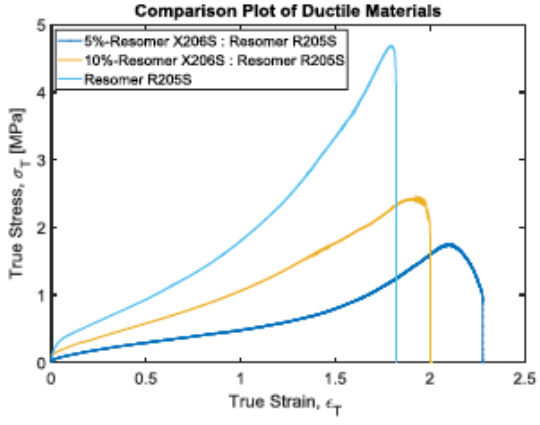

Fig. 32: A) An example of a stress-strain plot (displaying nominal and true data) for a sample of X206S, B) a stress-strain plot displaying the linear region and best fit curve used to determine the gradient of the slope- Young's modulus, and the Ultimate Tensile Strength (UTS), C) A true stress-strain curve comparison for Resomer L206S and its blends with X206S, D) A true stress-strain curve comparison for Resomer L206S and its blends with X206S.

The elastic behaviour of a polymer is described as when the stress in the material is proportional to the strain. In this portion of the stress-strain plot, if the load is removed, the material can return to its original state. This elastic behaviour is described by Young's modulus, also referred to as the stiffness of the material. In Figure 32B the Young's modulus for this particular specimen of X206S is approximately 420 MPa and the Ultimate Tensile Strength is 27.96 MPa. Yielding takes place as the material begins to deform plastically so therefore once the load is removed, the sample no longer returns to its original state. Yielding is occurring at the peak point of the linear portion of the stress-strain graph. Yielding point is also referred to as Ultimate Tensile Strength (UTS). In the elastic region, no necking occurs and if the load is removed the samples will revert to its original shape.

Table 3: Roundup of mechanical property data for the pure polymer and polymer blends

Polymer material	Elastic Modulus (GPa)	Average True Yield Stress (GPa)	Elongation at Ultimate Tensile Strength (%)
Resomer X206S	0.369 (±0.0528)	23.859 (±3.6941)	18.427 (±4.4550)
Resomer R205S	0.014 (±0.0041)	4.543 (±0.1297)	489.267 (±23.4730)
Resomer L206S	0.336 (±0.0338)	16.224 (±0.8019)	14.238 (±1.0785)
X206S: R205S (5:95)	0.003 (±0.0005)	1.467 (±0.2572)	596.799 (±77.4360)
X206S: R205S (10:90)	0.002 (±0.0003)	1.791 (±0.5837)	610.497 (±90.2663)
X206S: L206S (5:95)	0.438 (±0.0884)	20.472 (±3.2556)	12.538 (±1.5739)
X206S: L206S (10:90)	0.281 (±0.0759)	10.118 (±1.0498)	7.072 (±1.2170)

In the part of the graph that deviates from linearity, there is an increased stress required in plastic deformation until the ultimate tensile strength is reached. After the ultimate tensile strength is reached, the sample begins necking- the stress required to cause more plastic deformation decreases (this can be seen in Figure 32B after the UTS has been reached, as the graph begins to waver before fracture finally occurs). In Fig.22C it can be seen that the blends are more brittle in comparison to the more ductile blends in Figure 32D. In this stress-strain curve comparison (Figure 32C) it can be seen that the necking occurs within the sample after yielding. The polymer chains here become aligned with the direction of the load (vertical). Polymer chains are able to resist deformation along their grain as a

result of primary bond interactions. Elongation occurs as a result of this necking along the gauge length of the specimen. Resomer R205S (and consequently its blends) has a great elongation of almost 490% its original length at its ultimate tensile strength.

3.6. Finite Elemental Analysis

The computational methods used in this study is based around the principle of virtual testing. The designed testbed initiates at the virtual domain stage, where candidate designs of the stent (are imported into the testbed. The stent designs were created in a CAD Software (SolidWorksTM). Immediately after that, the material models stage helps define the behaviour of all components parts required for the stent study. The following are the set of stent structural parameters that will be determined to help understand the behaviour of the two stent designs based on the Resomer X206S material system: a) Radial recoil, longitudinal retraction, foreshortening and maximum stent stress.

Definition of stent structural parameters

Radial Recoil Percentage is a percentage of the ratio of change in internal diameter of the stent following deflation of the balloon with respect to the fully expanded internal diameter, it is expressed from the following equation:

$$R_{recoil} = \frac{ID_{expanded} - ID_{recoiled}}{ID_{expanded}} \times 100\% \quad (7)$$

Where ID = internal diameter. Over the three stages of stent deployment, the above can be represented graphically below:

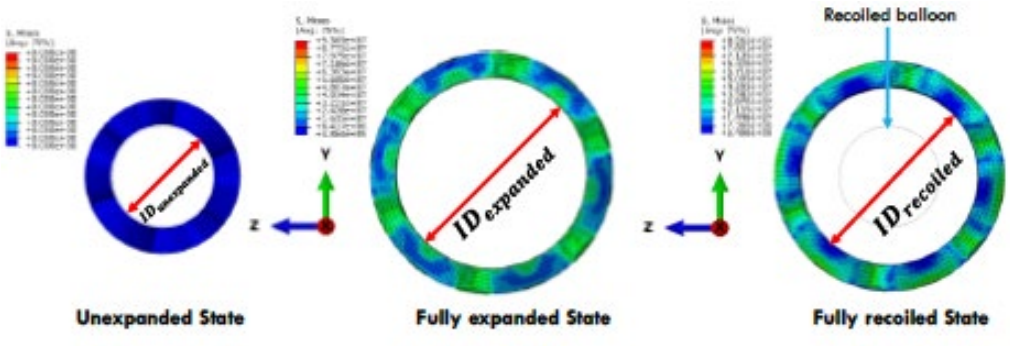

Fig. 33: Stages of stent deployment and their corresponding *internal diameters*

Longitudinal retraction is measure of the ratio of the change in stent length (axially) with respect to the original length of the stent. Mathematically, this quantity is defined thus:

$$L_{retraction} = \frac{L_{unexpanded} - L_{expanded}}{L_{unexpanded}} \times 100\% \quad (8)$$

Where $L_{unexpanded}$ and $L_{expanded}$ refer to the lengths of the stent in the unexpanded and expanded positions respectively. To illustrate this for the angular chevron stent element, **Figure 34** shows the side view of the stent.

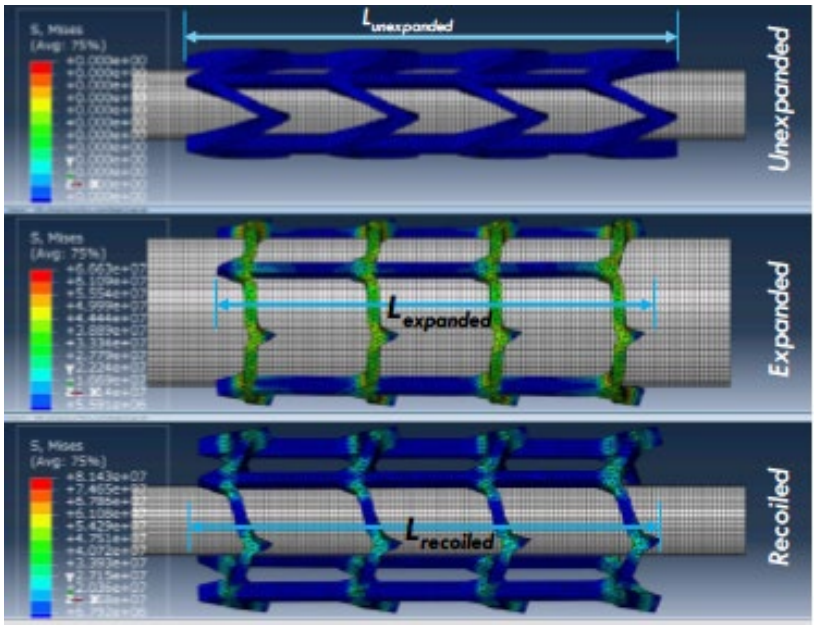

Figure 34: Stages of stent deployment and corresponding lengths, L of the angular chevron cell stent in unexpanded, expanded and recoiled positions.

Foreshortening is another structural stent parameter, related to the radial recoil percentage. *Foreshortening* refers to the ratio of the ratio of change in length (axially) of the stent between the recoiled position and the fully expanded position in comparison to the fully expanded length. It gives an indication of the lateral recoil of the stent following deflation of the balloon. Mathematically, it is expressed from:

$$F_{sh} = \frac{L_{recoiled} - L_{expanded}}{L_{expanded}} \times 100\% \quad (9)$$

where $L_{recoiled}$ is the length of the stent in the recoiled position.

Table 2: Results of the structural stent parameters for the two stent designs

S/No	Stent Name	Radial Recoil	Longitudinal Retraction	Fore-shortening	Maximum Diametral Strain	Maximum Stress (Mpa)
1	ANGULAR CHEVRON CELL STENT	9.94%	8.17%	2.60%	128.86%	81.43 Mpa
2	CURVED CHEVRON CELL STENT	10.45%	15.48%	5.40%	206.08%	71.7 Mpa

A good stent should aim to achieve the following:

1. Minimisation of the radial recoil percentage to within approximately 10%.

2. Minimisation of the longitudinal retraction percentage to within approximately 10%

3. Minimisation of the foreshortening to within approximately 10%

4. Maximisation of maximum stent stress, up to the yield stress of the stent material

5. Maximisation of the maximum diametral strain, up to the surgeon-desired strain.

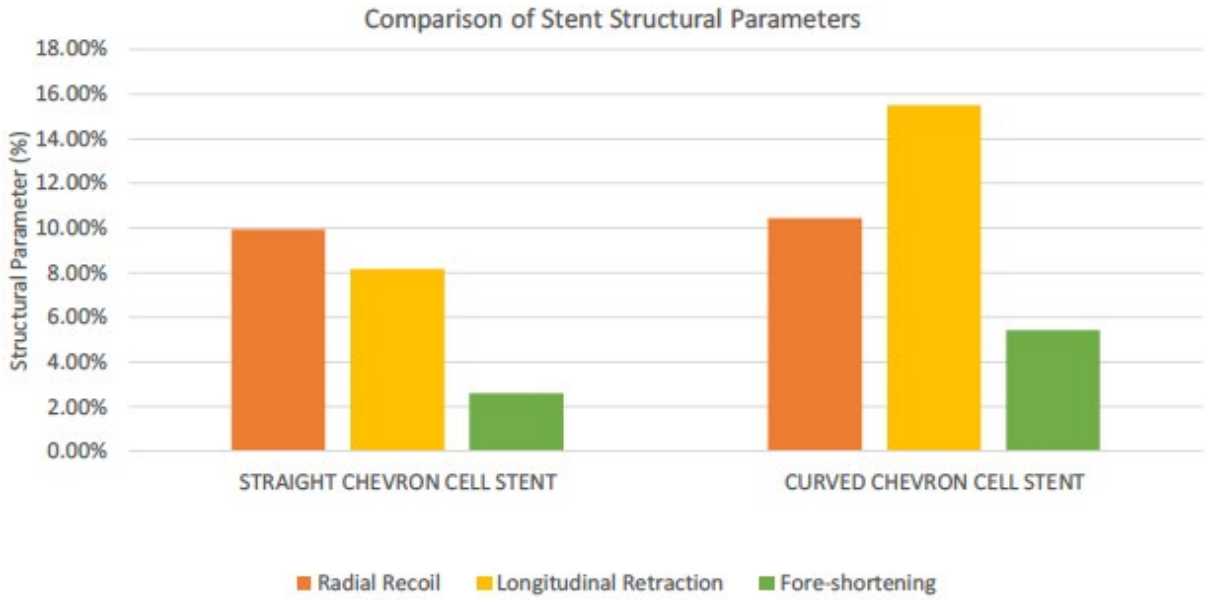

Fig. 35: Comparison of structural stent parameters

The stent structural parameters defined above were determined for the two stent designs based on the Resomer X206S material (**Table 3)**. Across all tested stent structural parameters, the angular chevron cell stent seems to out-perform the curved chevron cell stent. The former also meets with the requirements for a good stent design and compares favourably with metallic stents in all parameters. However, it experiences just over 100% maximum diametral strain, unlike the curved chevron cell stent which saw over 200% strain. The implication of this is that the curved stent will has a higher expansion potential and can be used for cases where large strains are required.

Histogram comparisons of the two stents and some of the structural stent parameters are given in **Figure 35**. The parameters for each stent design choice, must be minimized at 10% for both stent designs. As shown, the values obtained are within 10% except for the longitudinal retraction of the curved chevron cell stent.

The finite element analysis (FEA) has been carried out using two stent designs and material behaviour based on datasheet values for Resomer X206S. The results show excellent structural stent parameters, in line with expected stent parameters of commercially available metallic stents. The angular chevron cell stent seems to outperform the curved chevron cell stent in all assessed structural parameters, with exception of the maximum diametral strain. The methodology for such virtual testing of the stents has been established through this study. Future works will relate to undertaking similar virtual testing using the actual mechanical data generated from the experimental work in this project. Such studies will again show the suitability of the different stent materials developed in this work. FEA has given us a platform to assess the mechanical behaviour of the stent by combining complex geometric designs of the stents with complex material models, thereby offering us a means of assessing the functionality of our stents.

4. Conclusions

2 types of stents were developed and optimized, both made of nanofibers of biopolymer loaded with simvastatin for its stated antirestenosis properties. These virgin polymers demonstrated a very acceptable cytocompatibility and cytotoxicity profile while the cytotoxicity test methods showed that HPMEC cells proliferated with difficulty on nanofibers loaded with simvastatin. However, liberation studies serve to establish that the amount of simvastatin charged on NFs achieve the therapeutic dose.

Furthermore, the rabbit model offers the benefit of a quickly deployable and inexpensive model. It does not require a control group as each animal act as its own control, blocking comparison bias and allowing smaller numbers. The, in vivo studies suggest not convincing results for the stent made of PCD-CHT-SV but DES made of PU/SV must be further investigated.

Finally, the 3D printing technology developed by showed very promising results for the design and fabrication of personalized bioresorbable drug eluting stents (scaffolds) that can potentially revolutionize the area of implantable devices for the treatment of cardiovascular stents. The appropriate polymer selection along with the drug substance and the optimization of the printing technology can be further developed for patient treatment be using biodegradable stents that will disappear after 24 months while the artery will remain open without causing any potential risks to the patients'' health.

Description of the results obtained for the output in term of specific results category and specific result type

Specific results category And Specific result type	Modality of measurement	Description of the specific results
Knowledge Created/increased skills and Capacities	Already measurable: • 1 PhD Thesis (Lille 2019) • 2 article:Eur J Pharm Biopharm (2020) & Biomaterial Sciences (2021) • 10 presentations: Oxford Global (2019), CRS 2018, PharmSci 2019, Interpharm 2018, BioFit & Medfit 2019, Cellink 2018, Pfizer 2018, ICS3M 2019, Drug del. & Form. Summit Berlin 2020. Measured in June 2021: 1 PhD Thesis (Greenwich 2021) 1 review paper 2 research articles Measured on mid/long-term basis (2020-2024): The number of viewing/downloading and citation of the publications.	NEW STENTS#1 (Electrospinning) with dual therapeutic activity: antirestenosis with simvastatin (specific drug) loaded in nanofibers and anti-thrombosis with heparin like NFs. NEW STENTS#2 (3D printing) printed using FDM print techn. comprising of biocompatible and bioabsorbable polymers. Stents loaded with flavonoid drugs (quercetin & luteolin). The printed stents present controlled drug release, excellent mechanical prop. implantable in animals for clinical eval.
KnowledgeTechnological transfer	Already measurable: 1-1 meetings and discussions reports with the target groups contacted (see A.4 Target groups reached). Detailed description of the target groups contacted.	Meetings and discussions with targeted end groups (clinicians, companies). The developed technology and the new stent design should be adopted by medical companies who wish to develop

	Measured by the end of the project (June 2021): Additional 1-1 meetings and discussions reports with the target groups contacted (see A.4 Target groups reached). Detailed description of the target groups contacted Measured on mid-term basis (2020-2022): Transfer of technology of STENTS#1 and #2 with a company.	bioresorbable drug eluting stents with excellent clinical performance but also in a personalized manner where each stent can be adjusted to the patients' needs.
Socio-economic Increased business activity / capacity (new products, processes, services, techniques)	Measured on mid/long-term basis (2022-2024): • Number of new products adopted by companies. • Number of new products sold. • Increased profits of SMEs.	Increase of the competitiveness of SMEs via the use of the obtained outputs. STENTS#1 and #2 for biomedical applications.
Socio-economic Increased jobs	Measured by the end of the project: recruitment of PhD students and/or PostDocs in another company / university thanks to her/his work, experience and skills obtained in IMODE. Measured on mid/long-term basis (2022-2024): Direct job (job created in a company). If a concept of DES is transfer to a company, the direct job creation will be measured (recruitment of the PhD student in the R&D department or specific personnel in production/marketing as example).	The developed STENTS#1 and #2 will generate job creations.
Socio-economic Patent applications	Already measurable: 1 Invention disclosure related to STENTS#1	STENTS#1: 1 patent for DES

	has been submitted to the Tech Transfert Accelerator Network SATT-NORD (French side) in 2019. 1 patent related to STENTS#2 have been filed using patent solicitors in 2019 (Venner Shipley, London, UK) Measured by the end of the project (June 2021):1 additional patent filed Measured on mid/long-term basis (2022-2024): granted patents Measured on long-term basis (after 2024): Market use of the patents in the long run.	obtained by electrospinning → impossible to have patent after analyse of the invention disclosure STENTS#2: 1 patent for DES obtained by 3D printing

Communications

Reports and high impact publications	2 Papers : Kersani et al. (Eur J Pharm Biopharm) ; Hertault et al. (Biomat Sci) 2 reviews (Book Chapter)
Communications in European and/ or international events	**Communication (oral)** 1. Lopez, M; Kersani, D; Mougin, J; Tabary, N; Cazaux, F; Degoutin, S; Hue, B; Janus, J; Maton, M; Chai, F; Sobocinski, J; Blanchemain, N; Martel, B Study on the PVA stability of electrospun fibers for biomedical applications. 2nd Biomat Congress (BIOMAT 2017) Ambleteuse (France), June 12th - 16th, 2017 2. Mougin, J; Kersani, D; Hertault, A; Lopez, M; Degoutin, S; Tabary, N; Cazaux, F; Hue, B; Janus, L; Maton, M; Chai, F; Sobocinski, J; Martel, B; Blanchemain, N Simvastatin release from nanofibers covered stent and development of a rabbit iliac model for assessment of anti-restenosis bio-activity. ESVB 2017 Strasbourg (France), October 12th - 14th, 2017 3. Kersani, D; Lopez, M; Mougin, J; Degoutin, S; Tabary, N; Cazaux, F; Hue, B; Maton, M; Chai, F; Sobocinski, J; Blanchemain, N; Martel, B Simvastatin loaded chitosan/cyclodextrin polymer nanofibers-covered stent for restenosis prevention. International Conference on Processing & Manufacturing of Avanced Materials (Thermec'2018) Paris (France), July 8th -13th, 2018 4. Kersani, D; Lopez, M; Mougin, J; Degoutin, S; Tabary, N; Cazaux, F; Hue, B; Maton, M; Chai, F; Sobocinski, J; Blanchemain, N; Martel, B Coating of vascular stents with simvastatin loaded nanofibers by electrospinning for the prevention of restenosis and thrombosis. 29th Annual Meeting of the European Society for Biomaterials (ESB2018) Maastricht (The Netherlands), September 9th - 13th, 2018

	5. Degoutin, S; Kersani, D; Lopez, M; Mougin, J; Tabary, N; Cazaux, F; Hue, B; Maton, M; Chai, F; Sobocinski, J; Blanchemain, N; Martel, B Bilayer coating of vascular stent with electrospun bioactive nanofibers for the prevention of restenosis and thrombosis. 13th International Conference on Frontiers in Biomedical Polymers (FBPS) Tenerife (Spain), May 19th - 23th, 2019 6. Lopez, M; Kersani, D; Mougin, J, Tabary, N, Cazaux, F; Degoutin, S; Hue, B; Janus, L; Maton, M; Chai, F, Sobocinski, J; Blanchemain, N; Martel, M. Electrospinning of polyvinyl alcohol and polyurethane nanofibers for biomedical applications EuroCD 2019. 6th European Conference of Cyclodextrins Santiago de Compostela (Spain), October 2nd - 4th, 2019 **Communications (Poster)** 1. Kersani, D; Lopez, M; Mougin, J; Degoutin, S; Tabary, N; Cazaux, F; Hue, B; Jnaus, L; Maton, M; Chai, F; Blanchemain, N; Martel, B Drug-Eluting stents coated with nanofibers using electrospinning. 2nd Biomat Congress (BIOMAT 2017) Ambleteuse (France), June 12th - 16th, 2017 2. Mougin, J; Kersani, D; Hertault, A; Lopez, M; Degoutin, S; Tabary, N; Cazaux, F; Hue, B; Janus, L; Maton, M; Chai, F; Sobocinski, J; Martel, B; Blanchemain, N Simvastatin release from nanofibers covered stent and development of a rabbit iliac model for assessment of anti-restenosis bio-activity. ESVB 2017 Strasbourg (France), October 12th - 14th, 2017 3. Kersani, D; Lopez, M; Mougin, J; Degoutin, S; Tabary, N; Cazaux, F; Hue, B; Maton, M; Chai, F; Sobocinski, J; Blanchemain, N; Martel, B Drug-eluting stents coated with poly-cyclodextrin nanofibers. 5th European Conference on Cyclodextrins Lisbon (Portugal), October 4th - 6th, 2017 4. Kersani, D; Lopez, M; Mougin, J; Degoutin, S; Tabary, N; Cazaux, F; Hue, B; Janus, L; Maton, M; Chai, F; Sobocinski, J; Blanchemain, N; Martel, B Drug-eluting stents coated with poly-cyclodextrin nanofibers.

	18ème journée des Cyclodextrines Lens (France), November 28th - 29th, 2017 5. Kersani, D; Lopez, M; Mougin, J; Degoutin, S; Tabary, N; Cazaux, F; Hue, B; Maton, M; Chai, F; Sobocinski, J; Blanchemain, N; Martel, B Drug-eluting stents coated by simvastatin-loaded poly-cyclodextrin nanofibers: in vitro release study and in vivo preliminary evaluation. 19th International Conference on Cyclodextrins Tokyo (Japan), April 27th - 30th, 2018 6. Martel, B; Tabary, N; Degoutin, S; Kersani, D; Lopez, M; Mogrovejo, A; Palomino Durand, C; Gauzit, A; Cazaux, F; Janus, L; Neut, C; Blanchemain, N. Multi-shaped materials designed from cyclodextrin-based polyelectrolyte complexes 19th International Conference on Cyclodextrins Tokyo (Japan), April 27th - 30th, 2018 7. Kersani, D; Lopez, M; Mougin, J; Degoutin, S; Tabary, N; Cazaux, F; Hue, B; Maton, M; Chai, F; Sobocinski, J; Blanchemain, N; Martel, B Simvastatin loaded chitosan/cyclodextrin polymer nanofibers-covered stent for restenosis prevention. 46ème Journées d'Etudes des Polymères Gif-sur-Yvette (France), September 23th - 28th, 2018 8. Kersani, D; Lopez, M; Mougin, J; Degoutin, S; Tabary, N; Cazaux, F; Hue, B; Maton, M; Chai, F; Sobocinski, J; Blanchemain, N; Martel, B Development of nanofibers covered stent using electrospinning for the prevention of restenosis and thrombosis. Journée des Jeunes Polymèristes du Nord (JPN4) Lille (France), June 27th, 2019 9. Kersani, D; Mougin, J; Degoutin, S; Lopez, M; Tabary, N; Cazaux, F; Janus, L; Maton, M; Chai, F; Sobocinski, J; Blanchemain, N; Martel, B. Bilayer coating of vascular stent with electrospun bioactive nanofibers for the prevention of restenosis and thrombosis EuroCD 2019. 6th European Conference of Cyclodextrins Santiago de Compostela (Spain), October 2nd - 4th, 2019